USE OF A PULSED PHOTOMULTIPLIER TO MEASURE

THE LIGHT INTENSITY VERSUS TIME FOR

A SPARK DISCHARGE BETWEEN

ALUMINUM ELECTRODES

By

VERNON D. BROWN

Bachelor of Science
Arkansas State College
Jonesboro, Arkansas
1959

Master of Arts
Marshall University
Huntington, West Virginia
1965

Submitted to the Faculty of the
Graduate College of the
Oklahoma State University
in partial fulfillment of
the requirements for
the Degree of
DOCTOR OF EDUCATION
May, 1968

USE OF A PULSED PHOTOMULTIPLIER TO MEASURE

THE LIGHT INTENSITY VERSUS TIME FOR

A SPARK DISCHARGE BETWEEN

ALUMINUM ELECTRODES

Thesis Approved:

Francis C. Todd
Thesis Adviser

Fremont Harris

H. E. Harrington

Kenneth E. Wiggins

J. H. Blankenship

N. Durham
Dean of the Graduate College

ii

PREFACE

This work was undertaken at the suggestion of Dr. F. C. Todd who acted as the author's advisor and project supervisor. The purpose of the study is to investigate the emitted radiation as a function of time from dense aluminum plasmas. The dense plasmas were produced by an aluminum spark discharge inside a vacuum.

The author wishes to express his gratitude to Dr. Todd for his invaluable guidance and assistance in the completion of this work. The author is also grateful to Mr. L. J. Peery and Mr. W. C. Rhodes for the many discussions concerning the design and operation of the equipment used in this project.

The work was carried out under NASA contract number NASr-7 as administered through the Research Foundation, Oklahoma State University.

TABLE OF CONTENTS

LIST OF TABLES

LIST OF FIGURES

CHAPTER I

INTRODUCTION

Plasma physics is a study of the behavior of material in an ionized state. Macroscopic regions in the plasma must have zero net charge, although the microscopic regions have separated positive and negative charges.(1) This subject was studied extensively in the nineteenth century but not under this name. Examples of the earlier studies are lightning, glow discharges in tubes, and arcs. The basic concepts were found to apply to electrolytes, and these were included in the general field. It was not until 1930 that the accumulating subject matter was given the title of plasmas in a _Physical Review_ paper by Irving Langmuir and K. T. Compton.(2) As knowledge of the subject increased, the field of applicability also increased to include free electrons in solids as well as the huge plasmas that are the sun and the stars.(3) At present, the possibility of controlled power from nuclear fusion appears to be dependent on the containment of plasmas. With these extensions of the subject matter, the entire subject was eventually called plasma physics.

After showing the extent of the field of plasma physics, the subject matter of this thesis encompasses a rather small part of the entire subject. The subject matter deals with

the formation and phenomena in a spark between aluminum electrodes in a vacuum with the energy that is stored in a condenser. This general subject is very old. Benjamin Franklin produced sparks with his kite experiments. The early electrostatic machines were used to charge condensers and these charged condensers were used to produce sparks in a vacuum. My contribution of new information to this old subject is a consequence of developments in the field of plasma physics that have been made by a group at Oklahoma State University which is working on the subject with F. C. Todd.

The group at Oklahoma State is concentrating their work on dense plasmas. Two developments at the university have made possible the experimental work and the accompanying qualitative interpretation possible. One development is an analytical study of the "explosion," or expansion of a sphere of plasma. The sphere of plasma has a high energy density which results in a "gaseous" behavior and the external forces are removed by postulating an expansion into a vacuum. This study was made by R. E. Bruce in his dissertation for a Ph. D. degree.(4) The second development consisted of completing and operating a circuit to pulse a photomultiplier tube. With this equipment and a fast oscilloscope, the Tektronix 519, the rapidly changing intensity of the light is recorded during and immediately following the breakdown of a spark gap. The spark was between aluminum electrodes in a vacuum. My circuits limited the time

resolution of the intensity to 3/4 nanoseconds; i.e., 3/4 of one billionth of a second.

Objectives of the Problem

The work for this thesis is primarily concerned with the design and assembly of electronic equipment to apply an over-rated-voltage pulse to a photomultiplier tube. The objective is to obtain an increase in the tube sensitivity and to increase the power output from the tube. The completed circuits were tested by employing them to obtain the variation with time of the radiated intensity during the formation of a dense plasma. The dense plasma in this thesis was obtained by the breakdown of a spark gap between aluminum electrodes in a vacuum. The power for the spark came from the energy that was stored in a charged condenser.

The breakdown of a vacuum gap produces a small plasma with dimensions which depend on the energy stored in the condenser that supplies the spark. The plasma for study in this thesis was produced between two, spectroscopically pure, aluminum electrodes. The simple equipment for charging the condenser and obtaining the vacuum spark was assembled for the calibration of a spectrograph for the far-ultraviolet. The calibration films show intense lines near the short wavelength limit for our spectrograph which is 100 A°. The lines in the spectra have been identified and all specie of aluminum ions are required in the identifica-

tion down to Aluminum VI, which is from an aluminum ion with five electrons removed.

Some discussion is required of the characteristics and shape of the dense plasma that is formed by a high energy spark in a vacuum. The spark gap is very short, since the voltage is usually only about 10 kilovolts. The aluminum electrodes are rods which are about $\frac{1}{4}$ inch in diameter. One end of each rod is pointed with a tapered length of about 3/8 inch. The electrodes are mounted to be point to point, but the points are made to extend past each other so the tapered portion of the electrodes are parallel and are separated by about 0.1 to 0.5 mm. The spark may and occasionally is initiated at one or the other of the points of the electrodes. Usually the spark occurs between the parallel tapers. It is probably initiated at either of two positions: micropoints on the tapers which are rough finished, or at patches of insulation on the tapers. The points produce high local electric gradients. The patches of insulation produce breakdown by an effect which is called the Paetow effect.(5) In this effect, a charge is accumulated on the small patch of insulation which has an optimum size, neither too large nor too small. As the accumulated charge increases, the local fields increase until there is a small, local breakdown. This local breakdown supplies the ions and electrons for the breakdown of the gap, but also confines, by space charge, the electrode area for current conduction to a small region with a very high current density.

Breakdown of the gap produces an ionized path of high conductivity to conduct the current between the electrodes. The primary conversion of energy into heat occurs at the anode while the cathode is partially cooled by the combined field and thermionic emission of electrons.(6) As a consequence, the cathode is not as hot as the anode and is the source of the major portion of the emitted cloud of aluminum plasma. During and after breakdown, a dense cloud of aluminum vapor issues from a small area on the anode. This initially dense but rapidly expanding cloud is the primary source of the radiation that is observed by the photomultiplier tube. The initial form of the issuing cloud is hemispherical but numerical estimates indicate that the cloud will fill the gap during the period of observation until a cylindrical shape is observed at the end of observation. In this cloud of aluminum vapor, the current is apparently carried by a channel of small laterial dimensions, compared with the radius of the cloud. This channel becomes enclosed and more or less optically shielded by the hemispherical cloud that surrounds it.(7)

The photomultiplier tube is pulsed to record the voltage, current and light emission just after breakdown. As a consequence, the records do not show the rapid changes of the voltage and current during breakdown, but it does start to record these values immediately after breakdown is complete. In the recording of the emission of light, this delay is of negligible importance. The rule of thumb life-

time for an excited atom is of the order of 10^{-8} seconds, or 10 nanoseconds. As a consequence, no light is emitted during the breakdown and breakdown is followed by a gradual increase in the intensity of radiation. This gradual increase is observed.

If this general interpretation of the nature of the breakdown is correct, the work on this thesis provides some substantiation for a part of the work by Bruce on his thesis. In a completely analytical study, Bruce considered the expansion of a sphere of plasma which was initially hot and homogeneous. As the expansion proceeded, Bruce predicted the formation of a cold shell about the hot core.(4) This cold shell limits the radiation from the core that may be observed by photomultipliers. This thesis presents the evidence to support this prediction semi-quantitatively.

Theoretical Background

It has been shown by R. F. Post that the gain factor of a photomultiplier can be increased by pulsing it. The pulse voltage can be several times greater than the normal maximum operating voltage of the photomultiplier if the duration of the pulse is for only a few tenths of a microsecond.(8)

$$\ln I = KV \tag{1}$$

w h e r e I is the anode c u r r e n t, K = constant and V is the pulse voltage across the dynode resistors. The gain factor of the tube can be increased according to Equation 1 as much

as a hundred thousand times. Anode currents as high as seven amperes have been obtained from pulsed photomultipliers by Sidney Singer at Los Alamos while working with the United States Atomic Energy Commission.(9)

The photomultiplier was chosen as the detecting device as a consequence of its desirable characteristics and its accurate response during extremely short time intervals. The characteristics to be studied include the following:

1) Linearity, i.e., the voltage range over which the output current is proportional to the light input.

2) The rise time for a 4000 V pulse applied to an RCA 6199 photomultiplier is 3×10^{-9} seconds, while the transit time is 15×10^{-9} seconds when pulsed with a 4000 V pulse.(10)

3) The spectral response depends on the type cathode and on the scintillator, or filters, which are placed in front of the cathode.

By pulsing the photomultiplier for intervals of $.2 \times 10^{-6}$ seconds or less, corona and/or thermionic emission should present the only dark current problem.

The output from a photomultiplier can be fed into an oscilloscope, which permits the waveform of the output to be photographed.

CHAPTER II

INSTRUMENTATION AND DESIGN OF EQUIPMENT

Power Supplies

The power supplies, with the exception of the 300 volt supply, were designed by Mr. A. P. Brokaw under the direction of Dr. F. C. Todd. The basic assembly was done by Mr. Michael Potoczak. The author completed the assembly and made the power supplies operational.

The 1-750 volt d.c. bias supply is series regulated and is a reference for all other supplies on the chassis with the exception of the 300 volt unit which is of commercial manufacture. The low voltage 300 volt d.c. supply is a Dressen-Barnes model 22-106A and is available as a separate output. It supplies low voltage to the multivibrator and d.c. amplifier associated with the very high voltage supply.

The 1850 volt and the 1400 volt supplies are series regulated. They use the output of the 750 bias supply as a reference voltage.

The high voltage supply contains cathode-ray television tube power with its flyback transformer. It employs a feedback loop to control the output voltage in addition to the normal circuitry. The power supply is capable of producing voltages up to 22,000 volts. (11)

8

A schematic for the power supplies is shown in Figures 1 and 2.

The Pulsing Unit

The pulsing circuit with the exception of the hard tubes is a duplicate of the one used by Sidney Singer at Los Alamos when making measurements of rise and decay times of fast scintillators in 1953. (9) It is known as a "hard tube pulsing unit" and is common in radar circuitry. This type of unit was desirable since a pulse of 4 to 10 KV which was constant in magnitude was desirable.

The 2D21 thyratrons are triggered by applying a positive pulse approximately equal in magnitude to the negative bias on the control grid of the first 2D21. The output of the first 2D21 triggers the second 2D21 which in turn supplies a 1200 volt positive pulse to the control grid of the 4PR60B hard tubes. The hard tubes are completely saturated by this 1200 volt pulse and act as a closed switch during the duration of the pulse from the 2D21.

The 2D21 thyratron was selected to trigger the 4PR60Bs due to its fast rise time and uniform output while conducting. The conducting time or pulse length is controlled by the length of the coaxial cable connected to the plate of the 2D21s. The large plate voltage of 1850 volts is necessary in order to decrease the jitter between the thyratrons.

The pulse output from the hard tube circuit is kept constant by maintaining a pulse duration much less than the
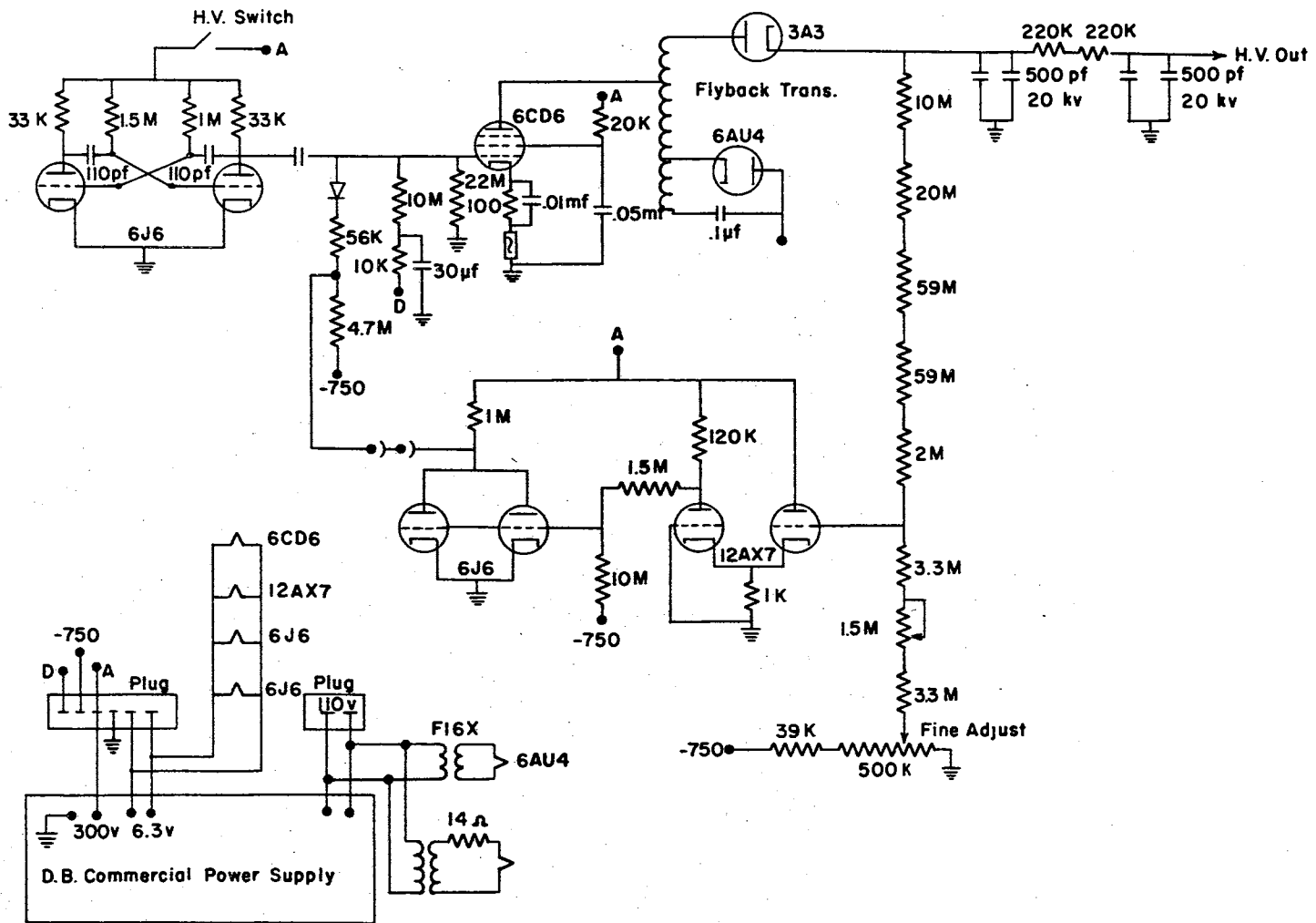
Figure 1. Schematic of High Voltage Power Supply for the Pulsing Generator
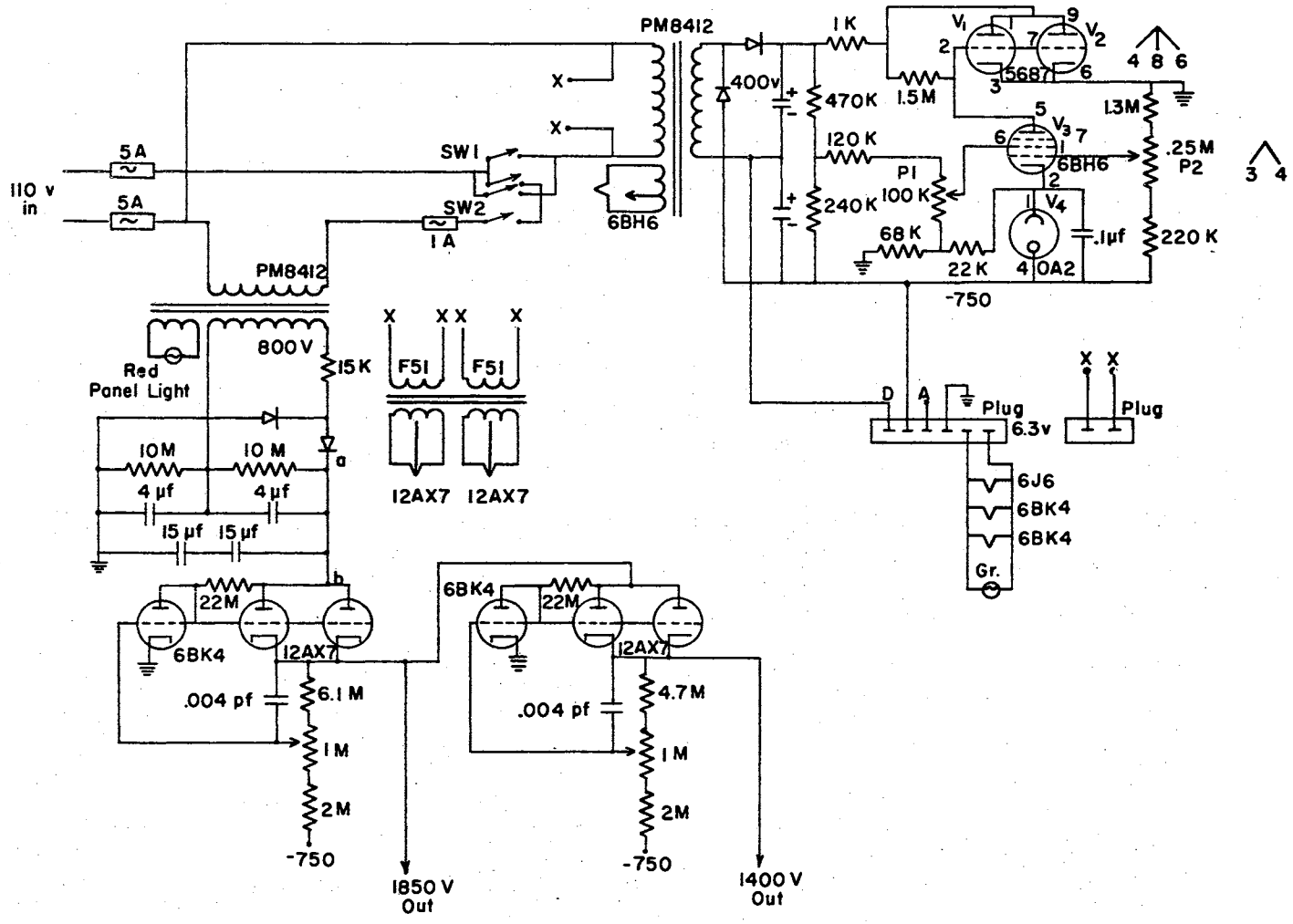
Figure 2. Schematic of Low Voltage Power Supplies for the Pulsing Generator

RC time constant of the circuit. The pulse current and voltage are determined by the voltage across the 15 μf capacitors.

Matched Impedance Feedthrough

As was mentioned in the introduction, the photomultiplier must be placed inside a vacuum chamber in order to view the far-ultraviolet radiation emitted from the aluminum spark. Before this could be accomplished matched impedance feedthroughs had to be designed and constructed. The vacuum feedthroughs had to match the impedance of the coaxial cable between the pulsing generator and the photomultiplier as well as the impedance of the coaxial cable between the photomultiplier anode and the oscilloscope. This problem was overcome by the design and construction of a simple yet efficient demountable matched impedance vacuum feedthrough.

Construction Steps

1) Machine a piece of brass to the specifications given in the drawing of Figure 6. This can be altered to fit any desired cable size as long as the mounting is on a flat surface.

2) Remove the insulation and ground shield from the proper length of cable. (12) If the center conductor is a multiple strand, remove the strands and replace them with a single strand of copper of the proper diameter using the equation
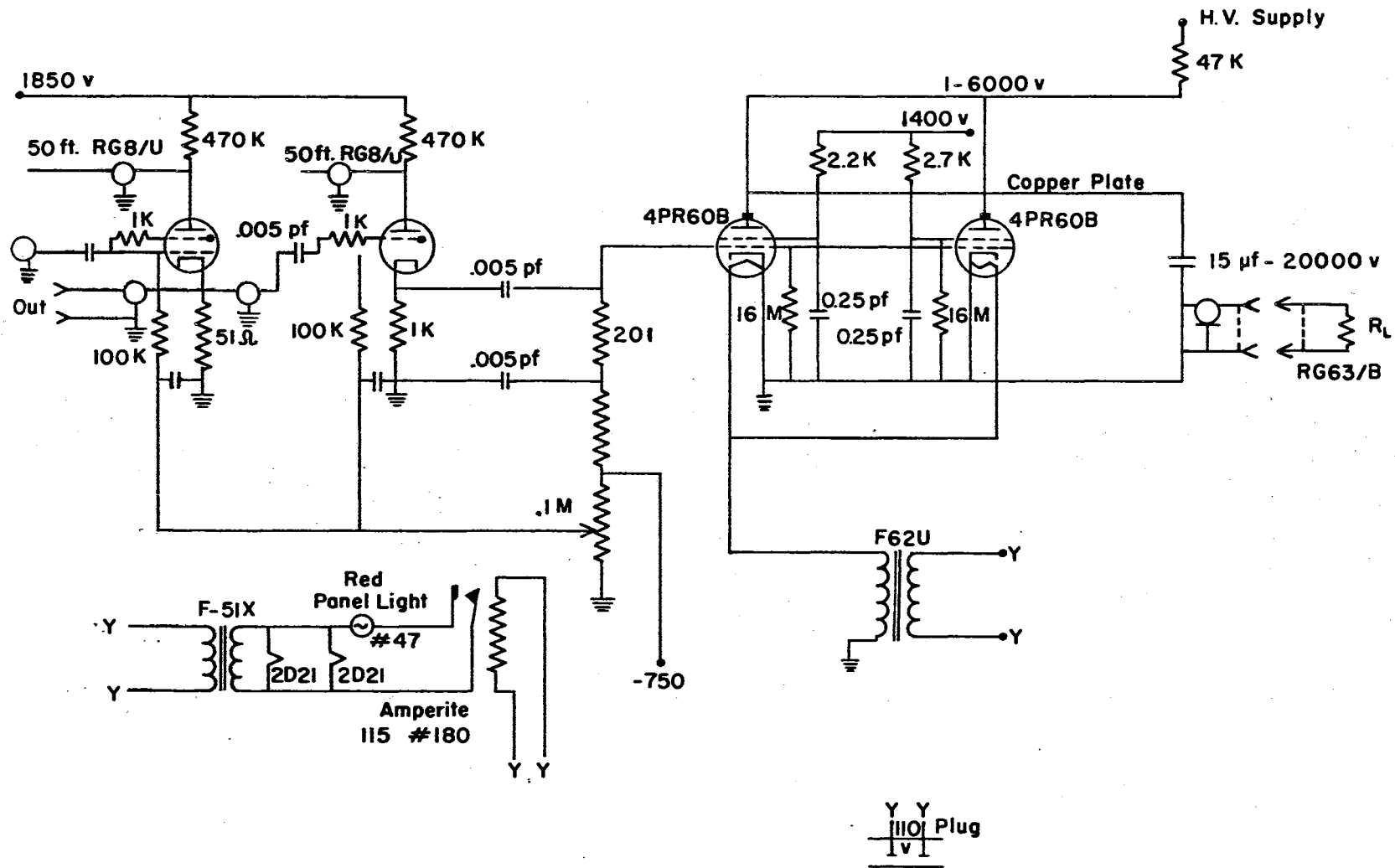
Figure 3. Schematic of Pulse Forming Circuit
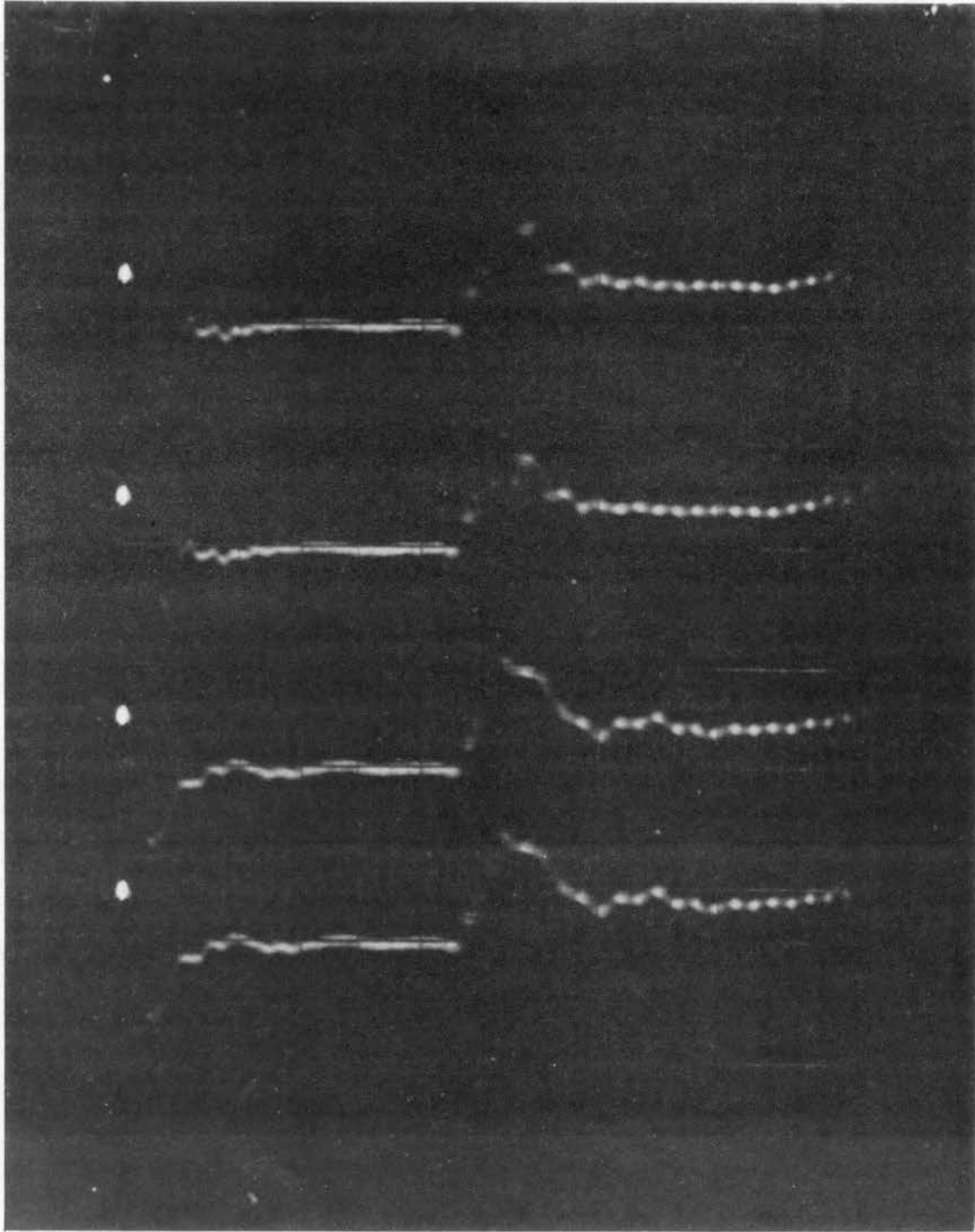
Figure 4. Pulse Shape Produced by the Pulsing Generator.

15 μf

I to 6 KV
Power Supply

$R_1 = 4700$ Ω

RG63B/U

to 519 Oscilloscope

$R_3 = 100$ Ω

$R_2 = 22$ Ω
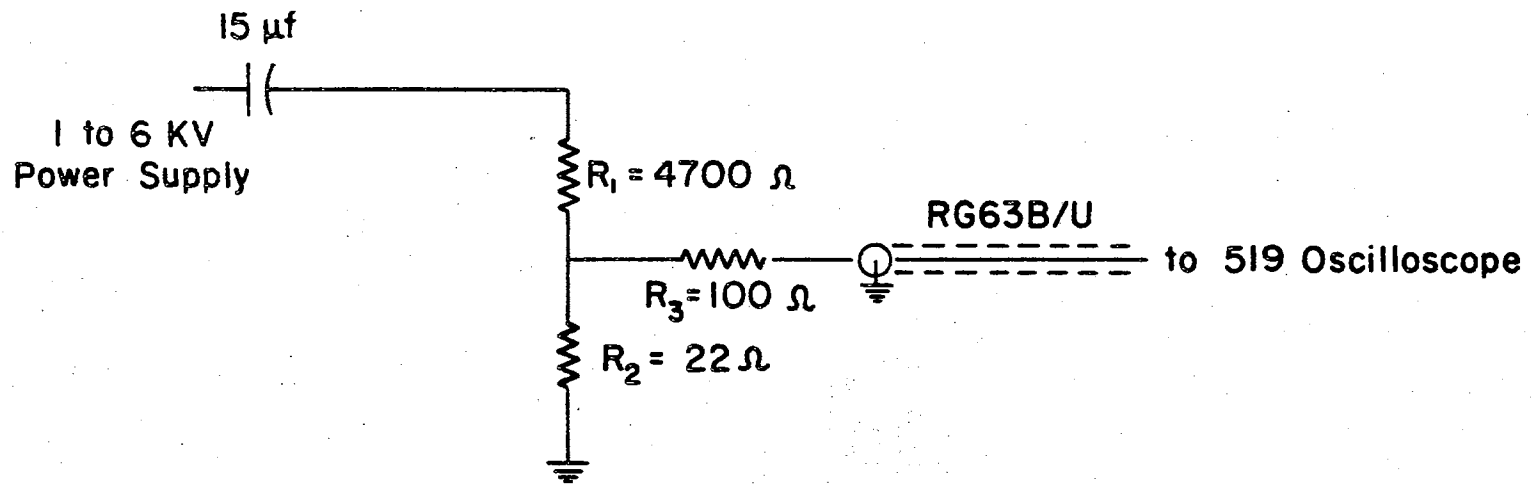
Figure 5. Schematic of Bridge Used to Make Photographs Shown in Figure 4

Figure 6. Cross Section of 50 ohm Matched Impedance Feedthrough

$$Z = \frac{138}{\sqrt{\text{dielectric constant}}} \log_{10} \frac{D}{d} \qquad (2)$$

where D = outer diameter of the dielectric material and d = outer diameter of the center conductor.

3) Now slide the piece of cable into the brass jacket and connect the brass to a test vacuum chamber. Crimp the feedthrough with a pipe cutter until the desired degree of vacuum is attained (12) (in this case it was 10^{-5} torr).

4) Place the proper cable connectors on the feed-through, (on this project type N connectors were used) and the feedthroughs are now operational.

Two different impedance feedthroughs are currently in use. A 50 ohm feedthrough constructed from RG8/U coaxial cable and a 75 ohm feedthrough constructed from a RG155/U coaxial cable.

<center>Calculation of Impedances</center>

50Ω Feedthrough

<center>dielectric constant = 2.3</center>
<center>center conductor outer diameter = 81 x 10^{-3} in</center>
<center>dielectric outer diameter = 284 x 10^{-3} in</center>

$$Z = \frac{138}{2.3} \log_{10} \frac{284}{81} = 74.4\Omega$$

75Ω Feedthrough

<center>dielectric constant = 2</center>
<center>center conductor outer diameter = 45.3 x 10^{-3} in</center>
<center>dielectric outer diameter = 284 x 10^{-3} in</center>

$$Z = \frac{138}{2} \log_{10} \frac{283}{45.3} = 74.4\Omega$$

The high voltage pulse from the pulsing generator was fed through the 75Ω feedthrough, while the output from the photomultiplier tube was fed through the 50Ω feedthrough.

The fundamental frequency of the pulse currently being used is 3.85 megacycles. The VSWR for the 50Ω feedthrough is shown in Figure 7. This is obtained by taking the difference between the load and the load plus feedthrough curves.

Photomultiplier

The next important problem to overcome was the wiring of the dynode bleeder resistor string. This was not a simple matter due to the fact that the photomultiplier was not being operated within the limits of the manufacturer's specifications.

The coaxial cable used between the pulsing generator and the photomultiplier had a surgent impedance of 75 ohms. This placed the restriction on the value of the total resistance of the dynode bleeder string of 75 ohms, since impedance matching is required in order to eliminate reflections.

The schematic for the dynode bleeder string is shown in Figure 8. The small value resistors between the first few dynodes were selected to help keep the noise to signal ratio low. Small ferrite cores were placed at all
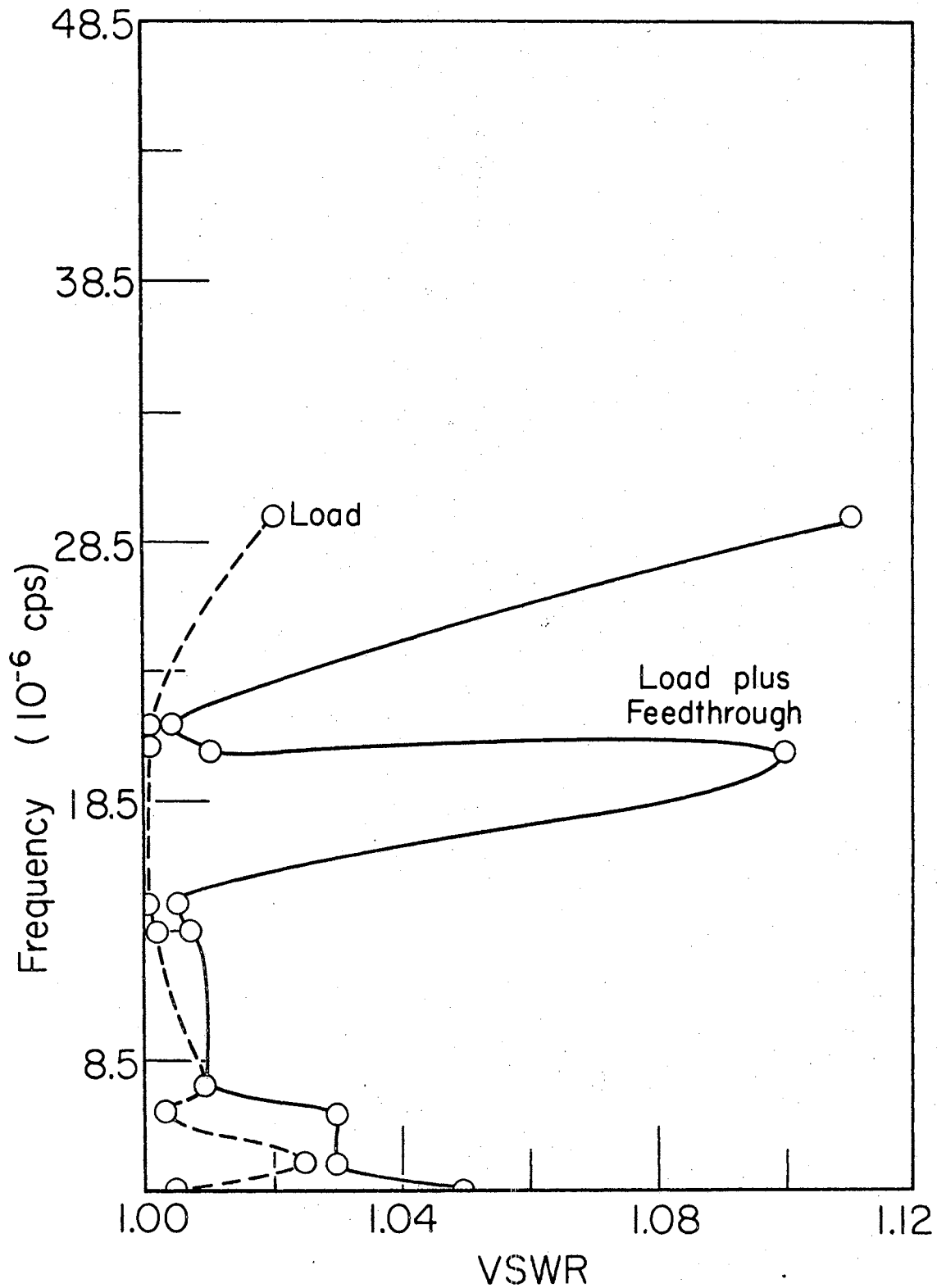
Figure 7. VSWR Versus Frequency Curves for the 50 ohm
Matched Impedance Feedthrough
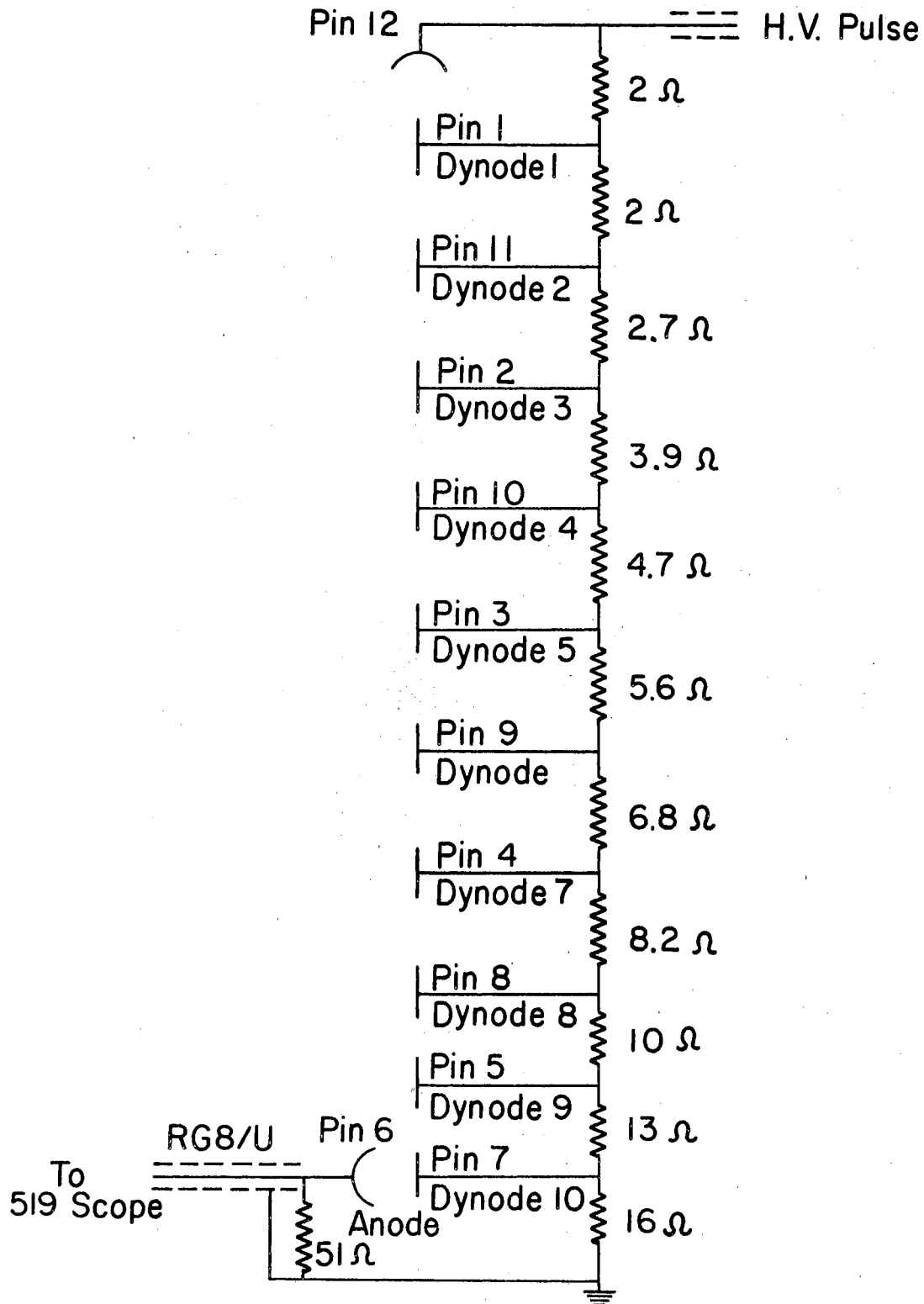
Figure 8. Schematic of the Dynodes Resistances for the
Photomultiplier

the connections of the dynode bleeder string to eliminate parasitic oscillations.

Operating at a pulse voltage much greater than 1200 volts (which is the maximum rated value by RCA) (10) corona and/or thermionic emission should present the only dark current problem. When operating an RCA 6199 photomultiplier under normal conditions, there are three sources of dark current: thermionic emission of electrons from the photocathode and other tube elements, ohmic leakage due to imperfect insulation, and regenerative ionization which causes instability at high dynode voltage. (13)

The Effect of Pulsing the Photomultiplier

The object in pulsing the photomultiplier was to increase the sensitivity or gain factor. A check on this was run by placing a uniform light source in front of the photomultiplier's cathode and varying the pulse voltage. It was found that the anode current increased from 5.43×10^{-3} amps to 326×10^{-3} amps when the pulse voltage was varied in 400 volt steps from 1800 to 4200 volts.

Triggering the Pulsing Generator to
View the Aluminum Spark

It was desirable to pulse the photomultiplier so that the photomultiplier would view the leading edge of the spark.

The timing of the spark discharge cannot be controlled more than a few seconds. The triggering of the pulsing unit
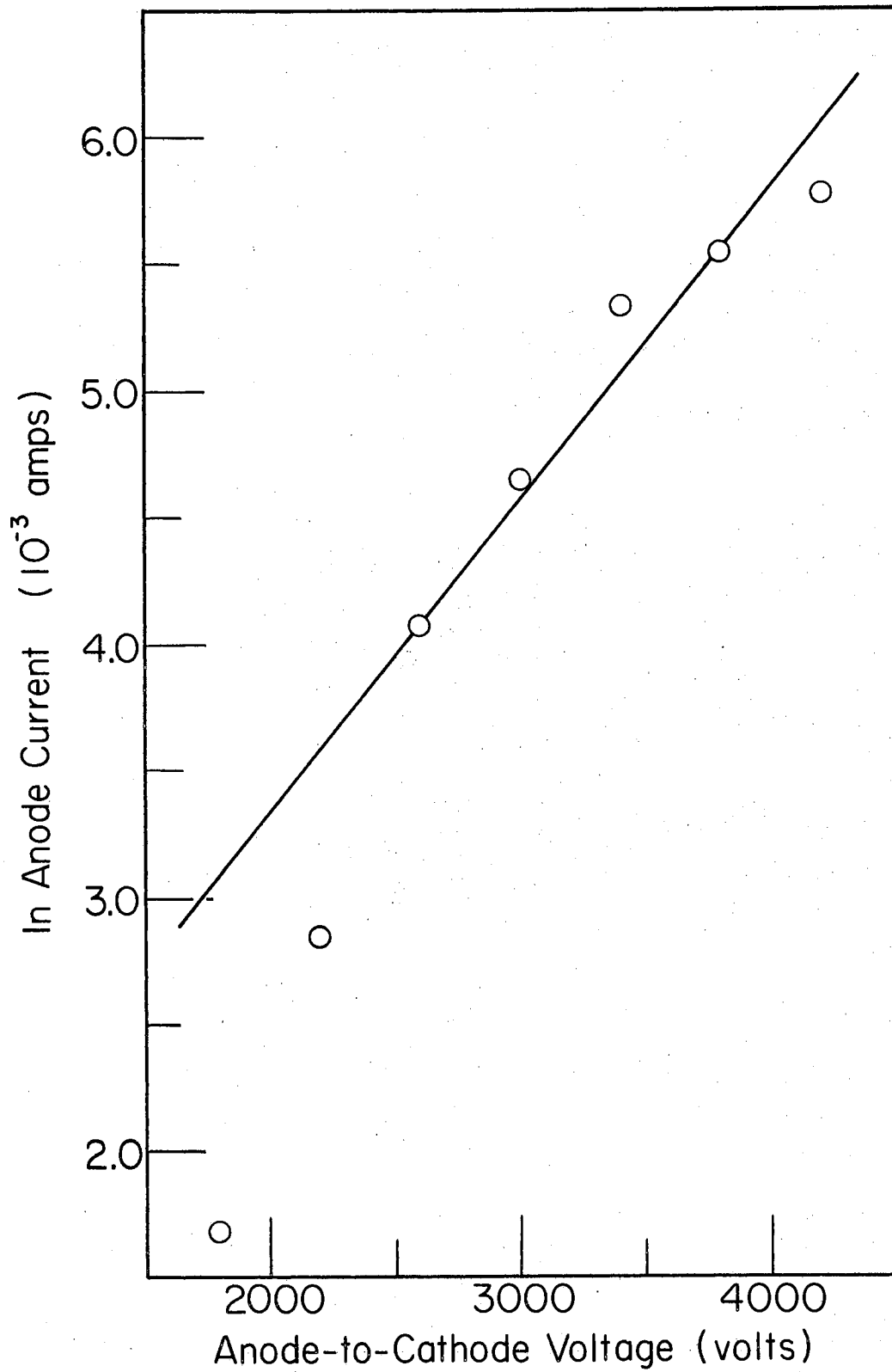
Figure 9. Log of the Photomultiplier Anode Current Versus
the Anode to Cathode Pulse Voltage

had to come within a few nanoseconds after the spark was
initiated. This could have been accomplished by at least
two methods. First, a secondary coil could have been placed
about the input cable to the aluminum spark. The induced
pulse from the coil could be applied to the control grid of
the first 2D21 thyratron. A second method and the one used
by the author consisted of placing a phototube a few centi-
meters from the aluminum spark. The phototube is also con-
nected to the control grid of the first 2D21 thyratron.
(The schematic for this triggering circuit is shown in
Figure 10.)
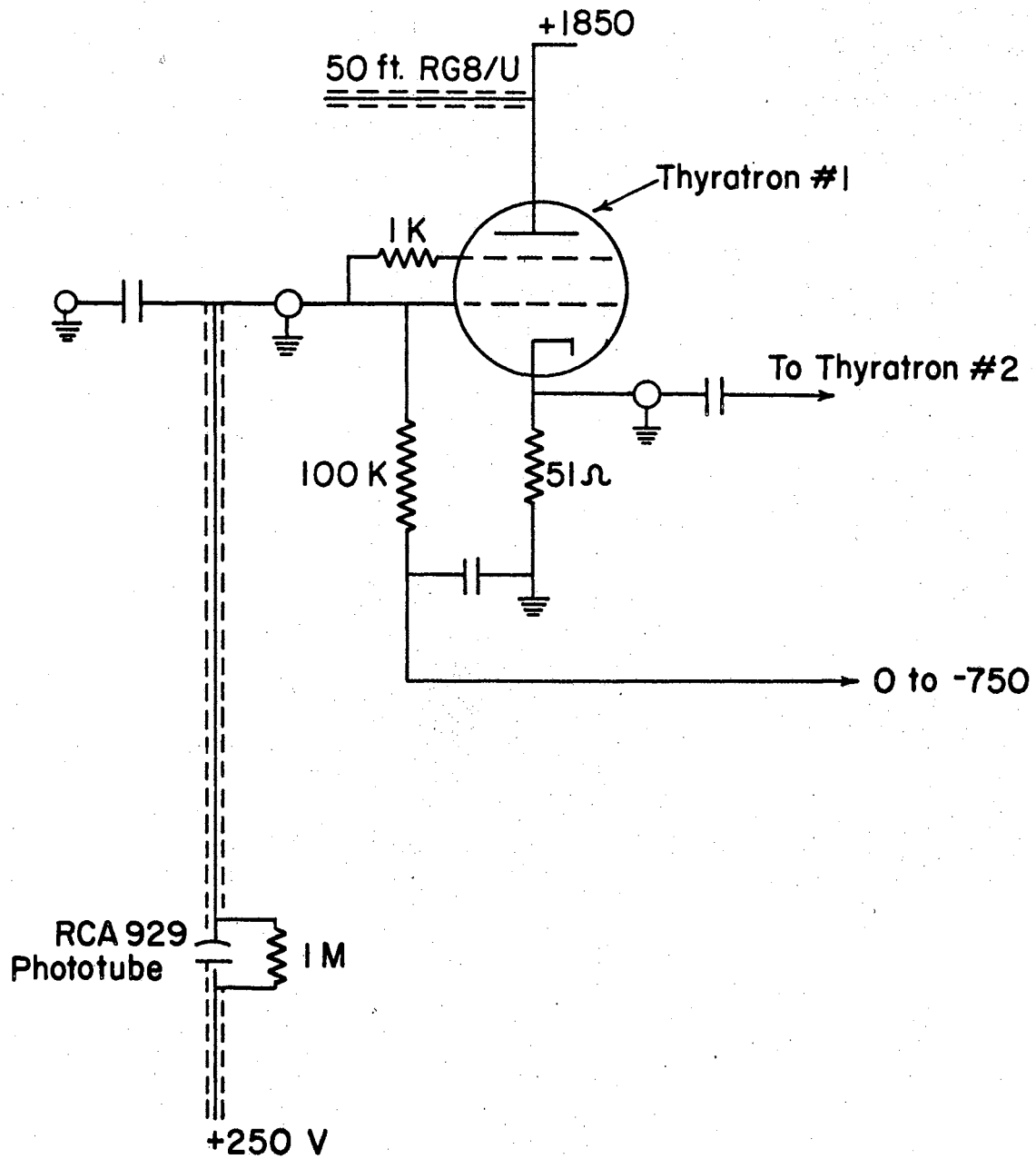
Figure 10. Schematic of the Pulse Generator's Triggering Circuit
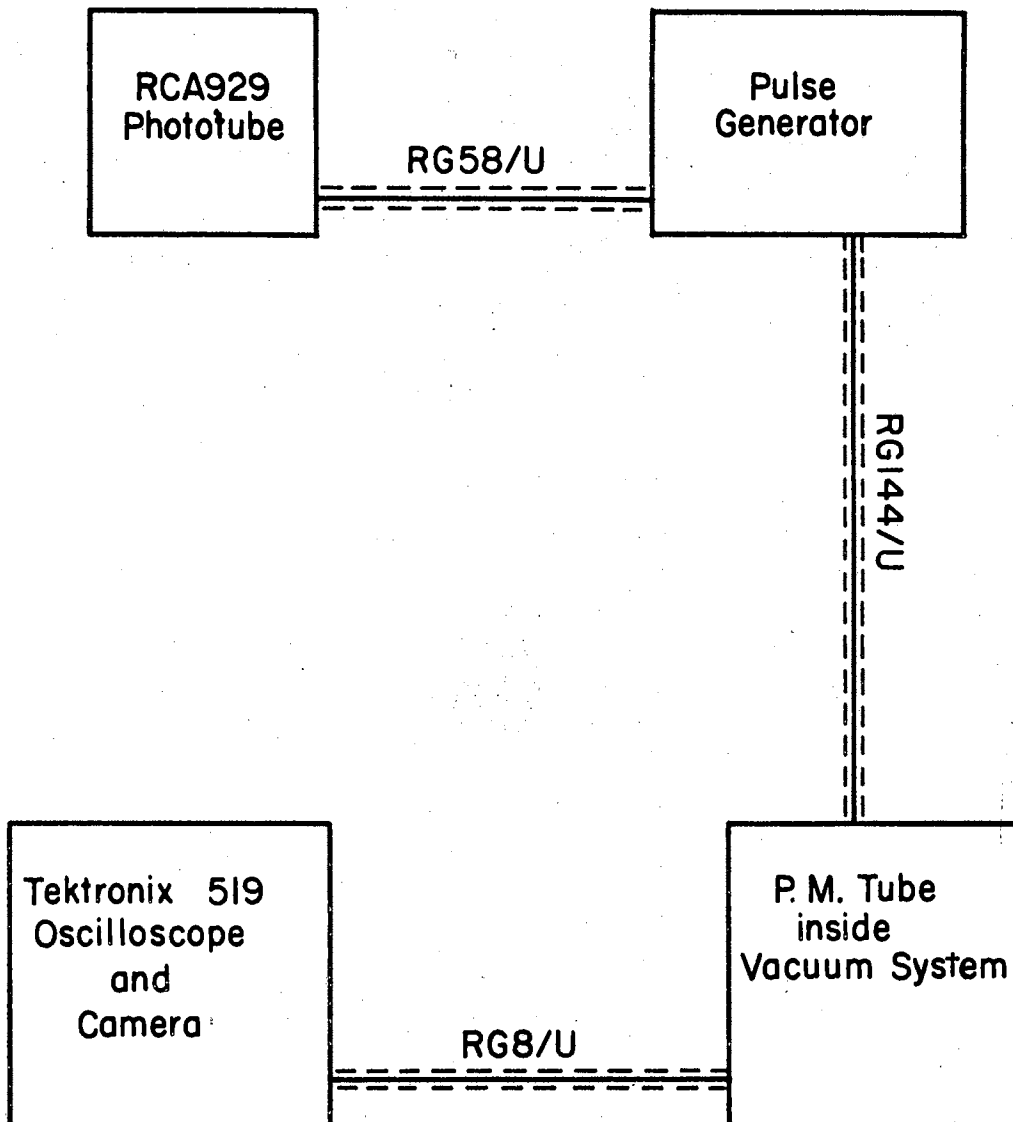
Figure 11. Block Diagram of the Data Collecting System

CHAPTER III

THE ALUMINUM SPARK

Spark Intensity Characteristics

Very little research work on the electric spark has
been published in the past fifteen years. The goal of the
author, as pointed out in the introduction, is to show how
the radiated intensity of light from an aluminum spark varies
with time.

The maximum light intensity increases rapidly with in-
creasing energy stored in the condenser (i.e., the intensity
is a function of the voltage, peak current, energy, induc-
tance, and electrode diameter).

For sparks between aluminum electrodes from 1/2 to 1/16
inch in diameter and at voltages above 5KV, the maximum
light intensity is inversely proportional to the square of
the diameter or to the cross-sectional area of the
electrodes. (7)

This is the one intensity controlling variable that
changes with each spark. Approximately 2×10^{18} atoms/spark
are lost by the electrodes, with each electrode losing close
to the same number of atoms. The intensity of emitted light
should decrease slightly with each spark after the electrodes
have been sharpened.

The voltage range across the capacitor was varied from 5KV to 10KV which in turn gave an energy value range of $E = \frac{1}{2}CV^2$, $E = \frac{1}{2} \, 10^{-7}$ farads x 25 $\overline{KV}^2$ = 1.25 joules to $E = \frac{1}{2} \, 10^{-7}$ farads x 100 $\overline{KV}^2$ = 5 joules, since the capacitance remained constant at .1 microfarad.

The inductance was determined from the resonant frequency of the spark circuit. The resonant frequency $f = 2$ x 10^5 cycles/sec.

$$f = \frac{1}{2\pi\sqrt{LC}} \; .$$

$$L = \frac{1}{4\pi^2 f^2 c} = \frac{1}{4 \times 9.98 \times 4 \times 10^{10} \text{ cycles}^2/\text{sec}^2 \times 10^{-7} \text{ farads}}$$

$$L = 6.32 \times 10^{-7} \text{ henries}$$

It was necessary to evaluate the inductance in order to calculate the peak current.

$$I_p = V(C/L)^{\frac{1}{2}} \quad (7) \qquad\qquad (3)$$

The peak current varied from $I_p = 5000V \, (\frac{10^{-7} \text{ farads}}{6.32 \times 10^{-7} \text{henries}})^{\frac{1}{2}}$

$5000 \, (\frac{1}{6.32})^{\frac{1}{2}}$ = $\underline{1.988 \times 10^3 \text{ amps}}$ to $I_p = 1000V \, (\frac{1}{6.32})^{\frac{1}{2}}$ = $\underline{3.976 \times 10^3 \text{ amps}}$.

Photomultiplier Output vs Time

Type Radiation Detected by Photomultiplier and Scintillator

Before looking at the actual photomultiplier output versus time, it is necessary to consider the spectral response of the photomultiplier and the transmission

and fluorescence characteristics of the scintillator screen.

The photomultiplier was an RCA 6199 ten stage multiplier with a common S-11 Cs-Sb lime-glass bulb photocathode. The anode pulse rise time is 2.8 nanoseconds when operated at low votages, but less than one nanosecond when operated at 4KV. (10) The absolute spectral sensitivity is shown in Figure 12.

A plastic scintillator of the Pilot Scintillator B Type made by Pilot Chemical was selected. The scintillator was placed over the cathode of the photomultiplier to absorb the ultraviolet radiation ranging from far to near ultraviolet and to re-emit it by fluorescence at a wavelength within the spectral sensitivity of the S-11 photomultiplier cathode. By checking Figure 13, the fluorescence spectrum of the scintillator, one sees that the maximum fluorescence is approximately 4100 angstroms. (14) This is near the maximum sensitivity of the S-11 photomultiplier cathode.

The absorption by the scintillator is small, .05, and remains constant between 3945 angstroms and 5300 angstroms. The data in Table I and the graph in Figure 14 show the rapid decrease in the transmission of the scintillator for wavelengths between 3910 angstroms and 3800 angstroms.

Intensity Versus Time Measurements

The radiation intensity versus time from over 200 aluminum sparks have been recorded by the author. The
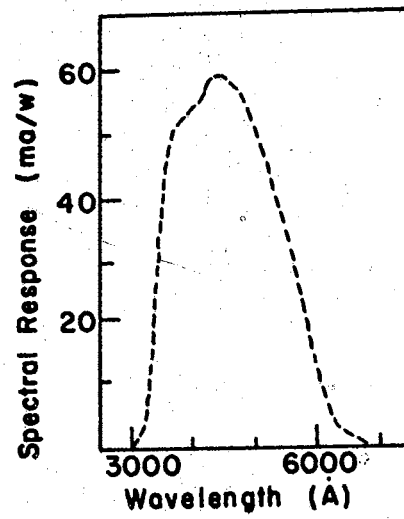
Figure 12. Spectral Response Versus Wavelength Curve for a S-11 Photocathode
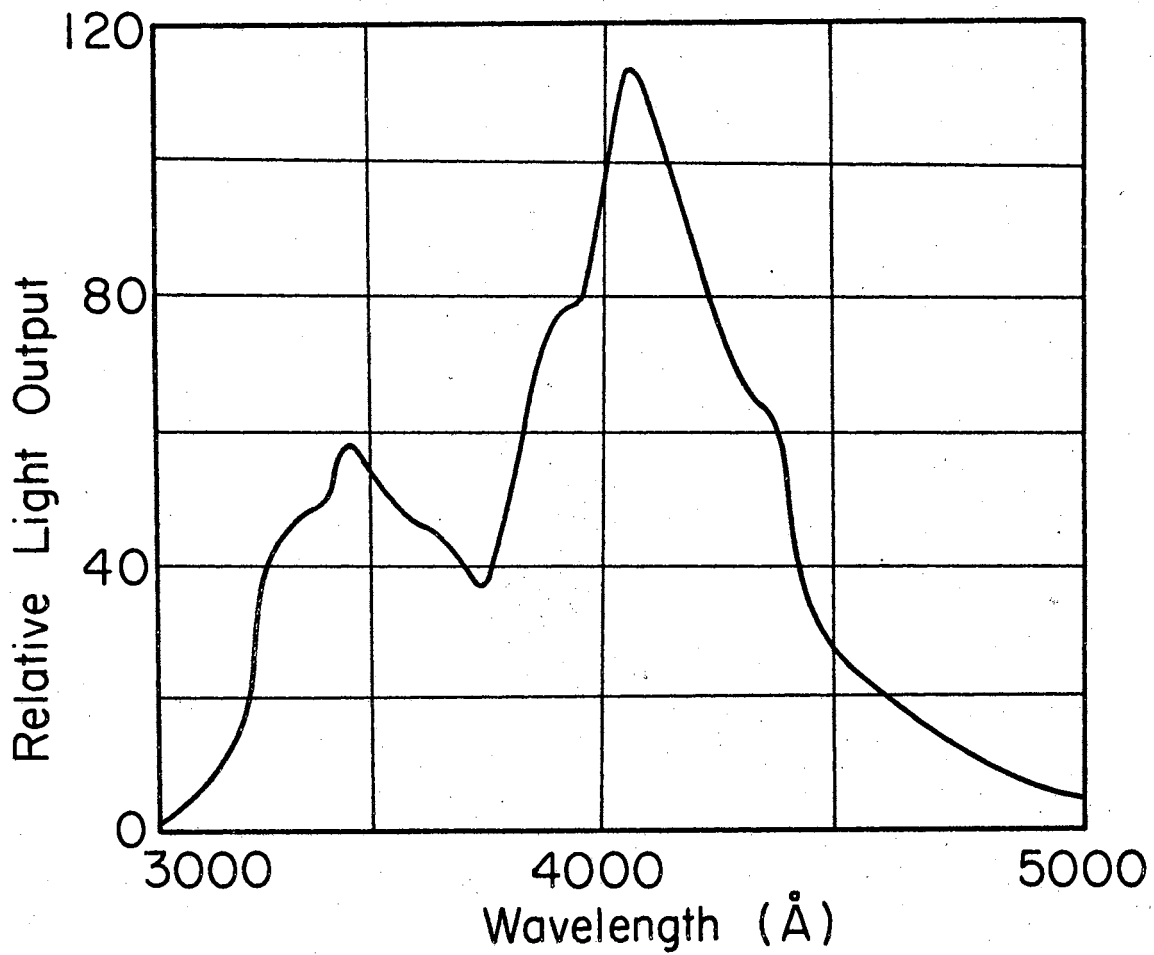
Figure 13. Fluorescent Spectrum for the Pilot Scintillator
B-Type (14)

TABLE I

TRANSMITTANCE OF PILOT SCINTILLATOR B-TYPE BETWEEN 5300 Å AND 3800 Å.

$$A = \log P_0/P = .05$$

$$P_0/P = 1.12 \quad P = 1/1.12 = 89.4\%$$

$$5300 \text{ Å} \quad \text{to} \quad 3945 \text{ Å}$$

A	λ	P_0/P	P
10	3910	1.26	79.4
12	3900	1.318	75.9
15	3890	1.41	70.9
20	3875	1.584	63.2
25	3870	1.78	56.2
30	3862	1.993	50.2
35	3855	2.24	44.7
40	3846	2.518	39.5
45	3840	2.82	35.5
50	3835	3.16	31.6
60	3830	3.98	25.1
70	3823	5.0	20.0
80	3815	6.32	15.8
100	3800		0
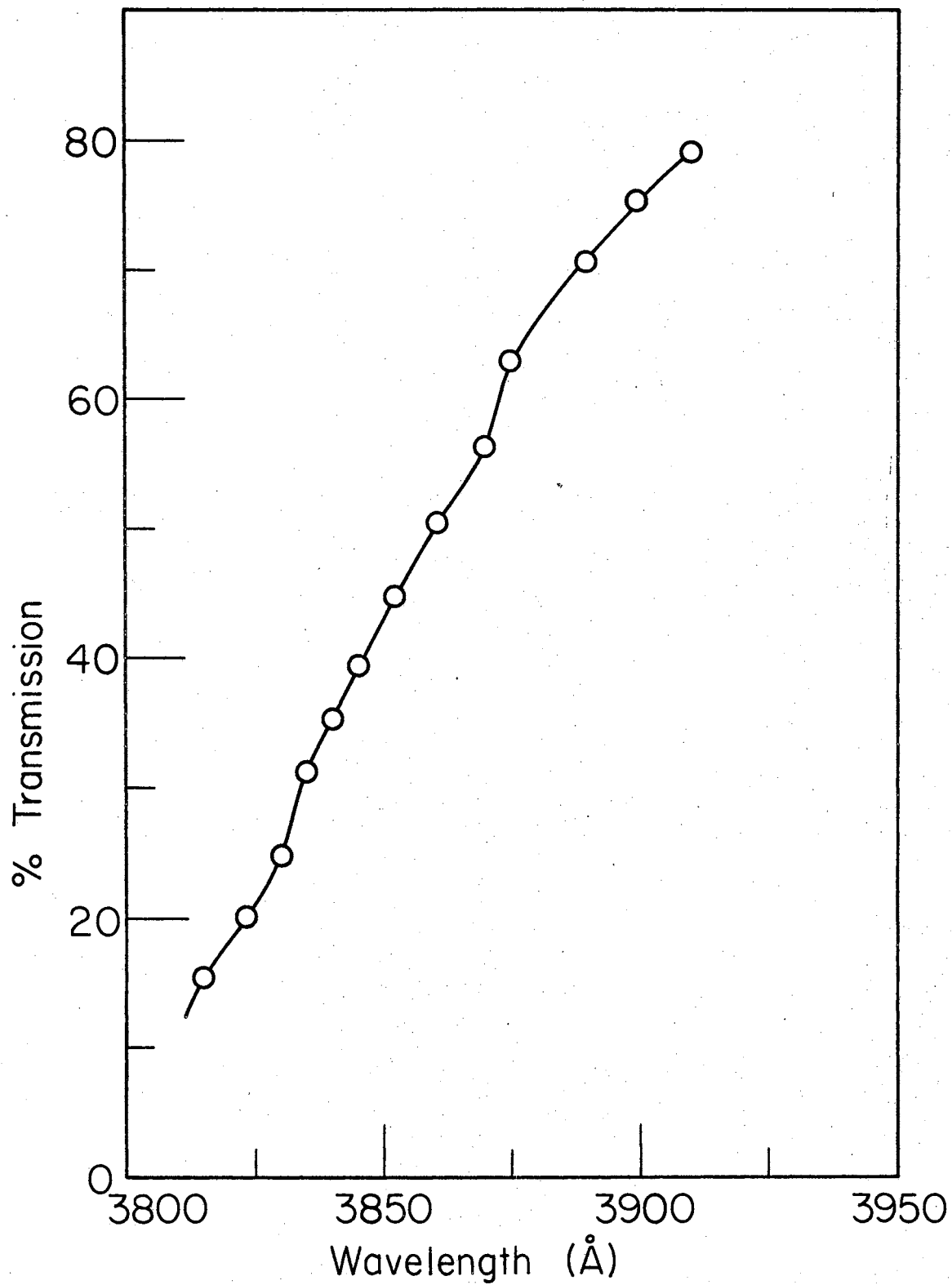
Figure 14. Transmission Cut-off of Pilot Scintillator in Front
of the Photomultiplier's Cathode

relative intensity versus time was filmed at different oscilloscope scan speeds ranging from 5 to 100 nanoseconds per centimeter. The pulse voltage was kept constant at 4000 volts. The films were made both with and without the scintillation screen over the face of the photomultiplier.

The voltage across the sparking capacitor varied from 5 KV to 10 KV with most of the sparks occurring at 10 KV depending on the position and sharpness of the aluminum electrodes. No two sparks gave identical radiation intensity versus time curves since the physical conditions for each spark were different. There was, however, a predominant high intensity versus time recorded at the leading edge of the pulse. It varied in length from about 3 to 5 nanoseconds. A sharp decrease in intensity followed with smaller oscillations occurring during the next forty to seventy nanoseconds.

The intensity variation near the beginning of the spark was more pronounced without the scintillator over the face of the photomultiplier. This shows that the ultraviolet radiation was quite intense near the beginning of the spark when one considers that the scintillator is re-emitting in all directions. Past the eight nanosecond period of the spark, the radiation intensity versus time seems to remain almost constant for the next 150 nanoseconds. The ultraviolet radiation was still evident during this time period but much smaller in relative proportion.

The graphs of the radiation intensity versus time from eight selected sparks are shown in Figures 15 through 22. Figures 16, 18, 20, and 22 show the recorded radiation intensity versus time curves with the scintillator in front of the photomultiplier cathode, while Figures 15, 17, 19, and 21 show the recorded radiation intensity versus time curves without the scintillator positioned in front of the photomultiplier cathode.

<p style="text-align:center">Voltage and Current Monitor</p>

The voltage and the current were both monitored during the same time period as the radiation intensity versus time films were photographed. The major concern was to ascertain if the power across the spark remained practically constant during the sharp oscillation in the radiation intensity near the beginning of the spark. Figures 23 and 24 will show, however, that the power did remain about constant during the time in question.

It was fairly simple to monitor the current with a single turn around the positive lead between the .1μf sparking capacitor and the aluminum electrode. This procedure gave the variation in the current with time. The synchronization of time was assured by using the proper coaxial cable length between the induction turn and the oscilloscope. This length gave the same pulse transit time as the transit time of the electrons through the photomultiplier plus the travel time of the pulse from the photomultiplier's anode to the oscilloscope.

Figure 15. Detected Radiation Intensity Versus Time from the Aluminum Spark Without the Scintillator in Front of the Photomultiplier's Cathode
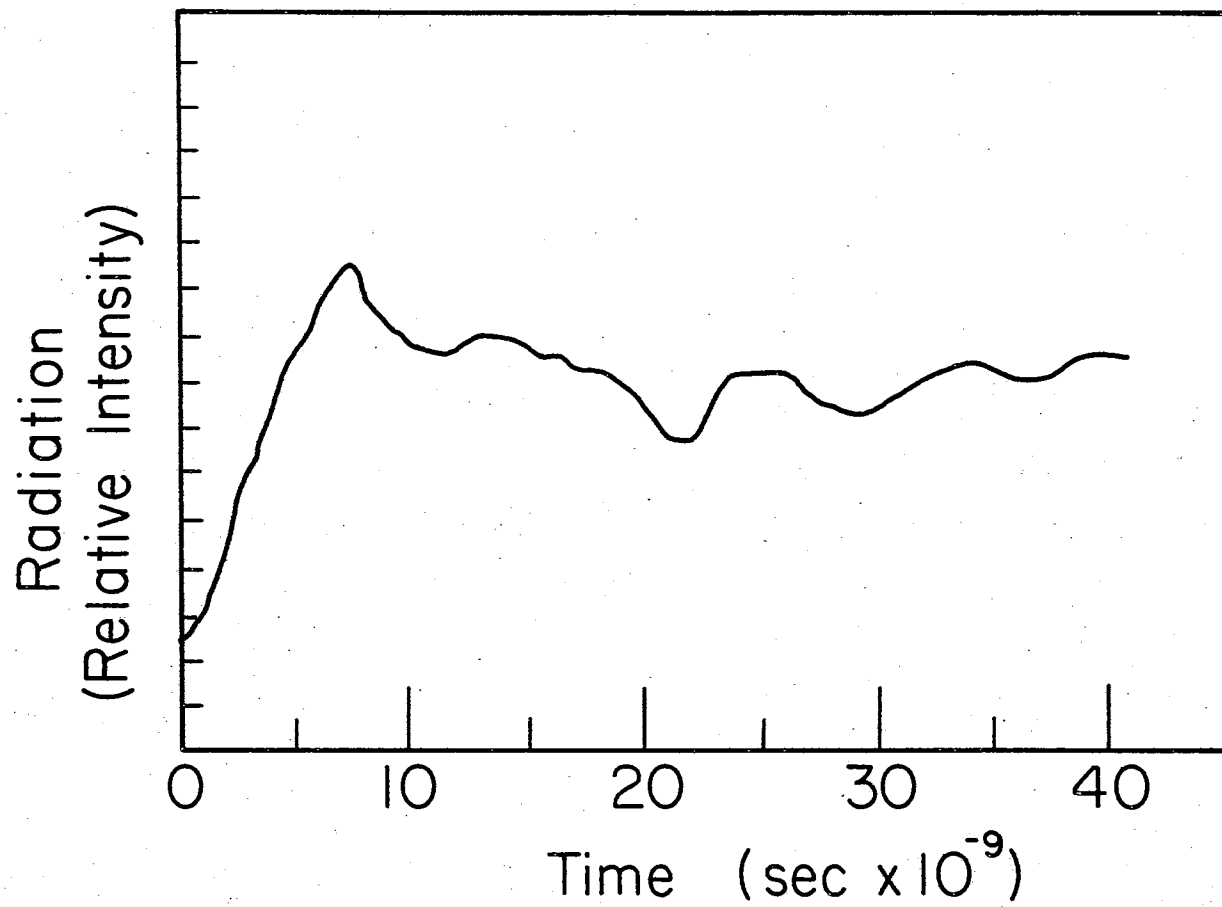
Figure 16. Detected Radiation Intensity Versus Time from the Aluminum Spark
with the Scintillator in Front of the Photomultiplier's
Cathode
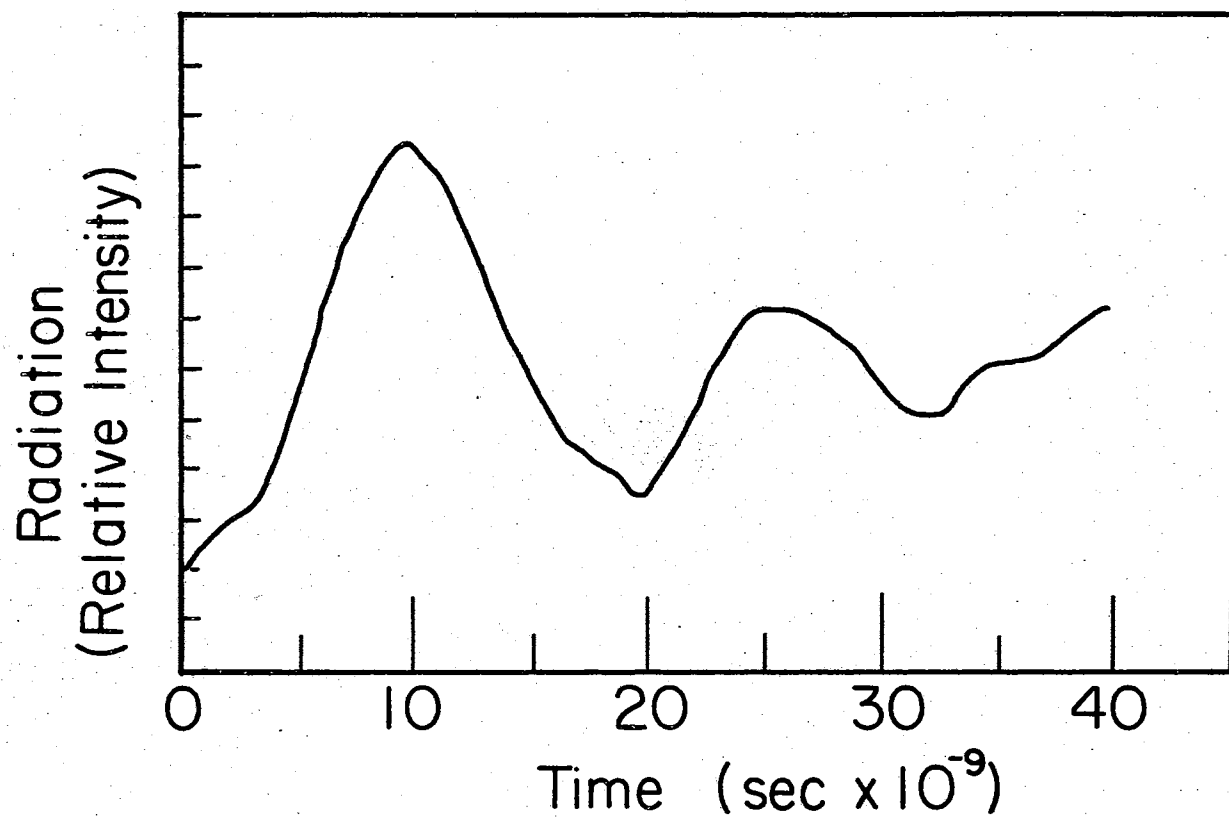
Figure 17. Detected Radiation Intensity Versus Time from the Aluminum Spark
Without the Scintillator in Front of the Photomultiplier's
Cathode
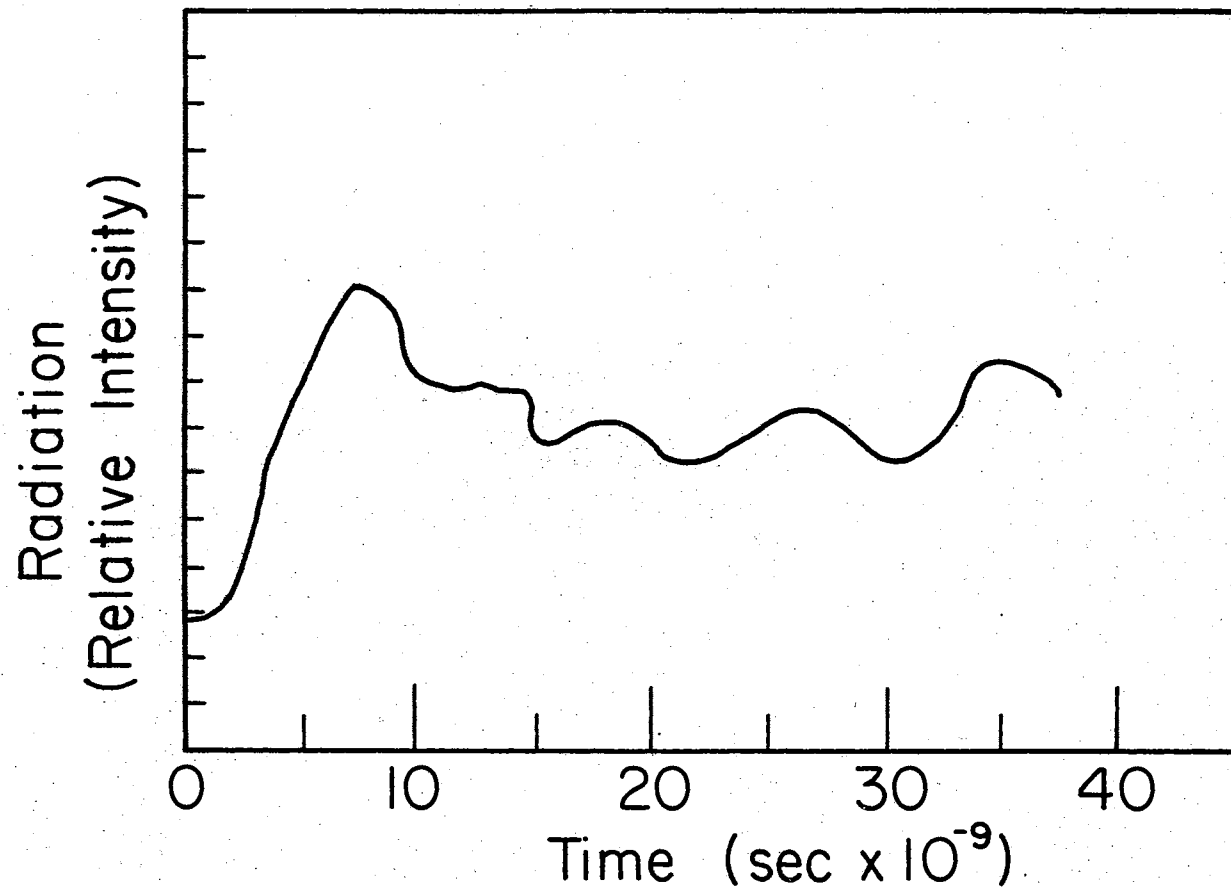
Figure 18. Detected Radiation Intensity Versus Time from the Aluminum Spark
With the Scintillator in Front of the Photomultiplier's
Cathode
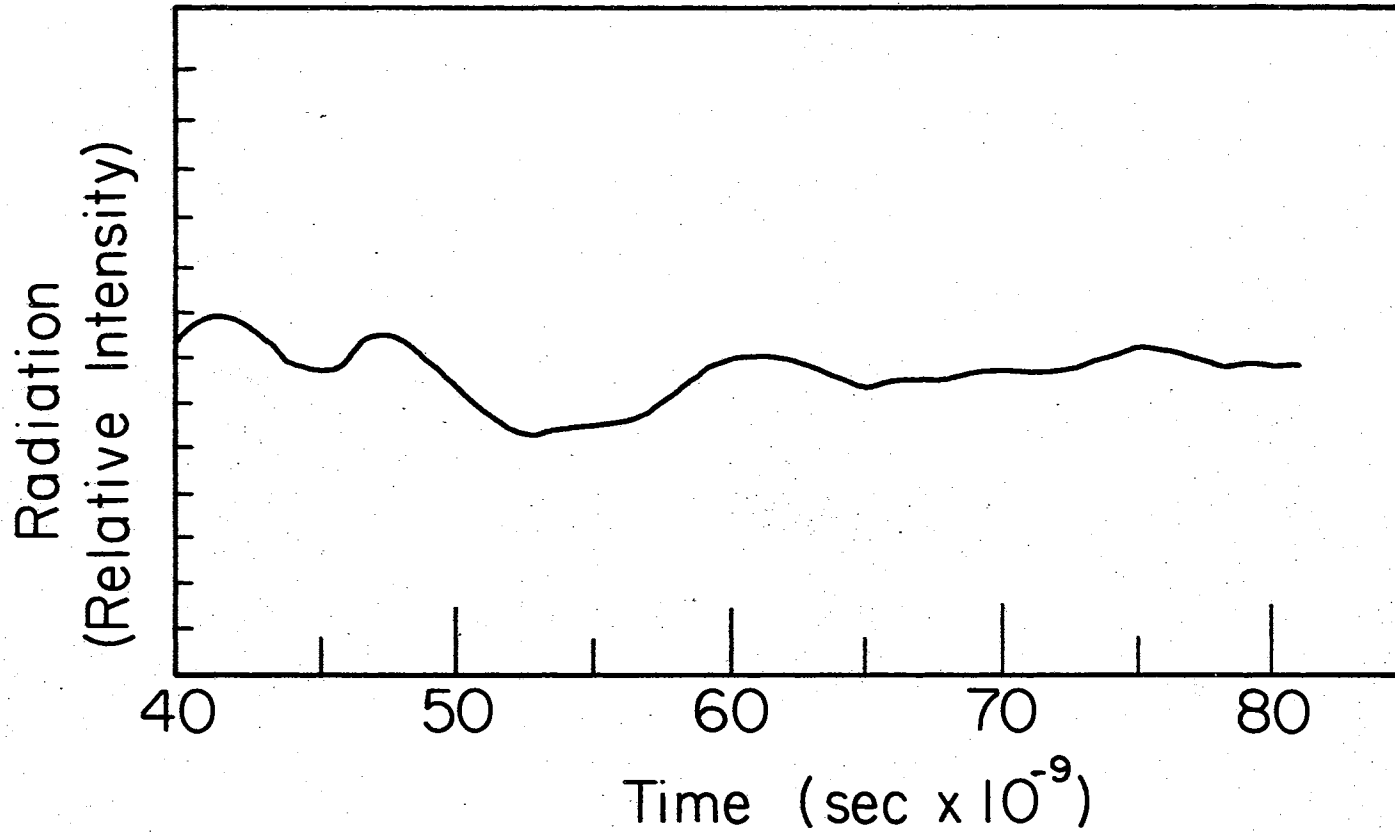
Figure 19. Detected Radiation Intensity Versus Time from the Aluminum Spark Without the Scintillator in Front of the Photomultiplier's Cathode
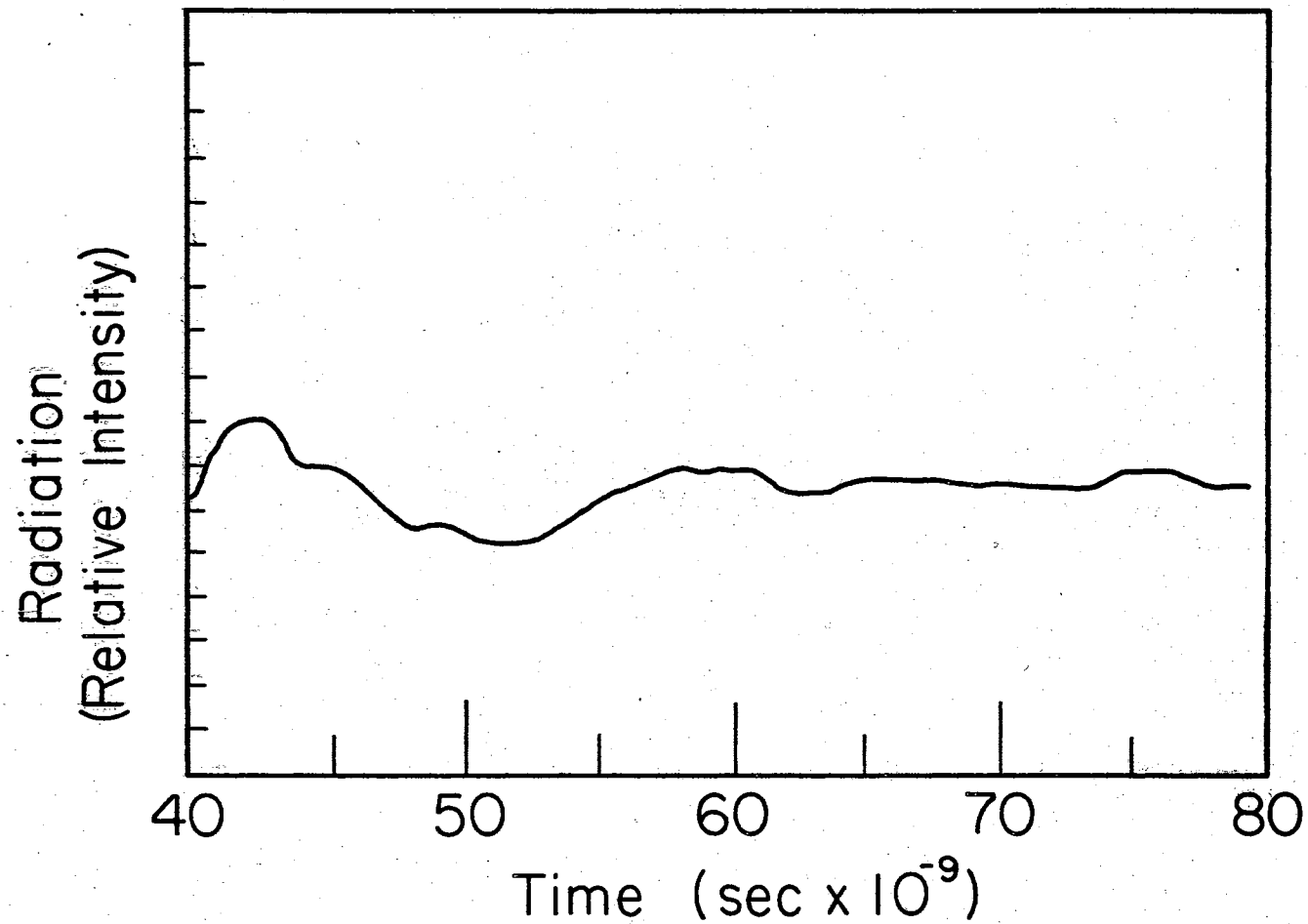
Figure 20. Detected Radiation Intensity Versus Time from the Aluminum Spark With
the Scintillator in Front of the Photomultiplier's Cathode

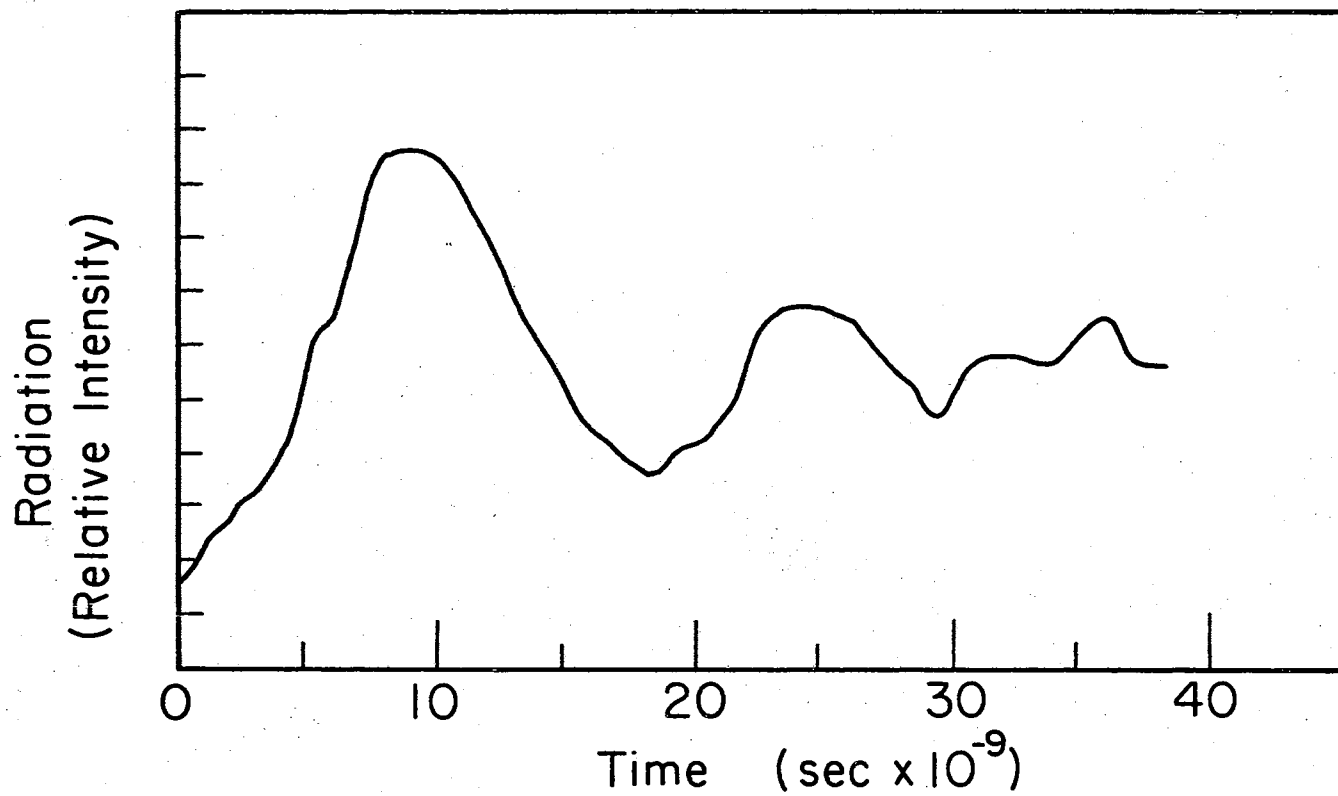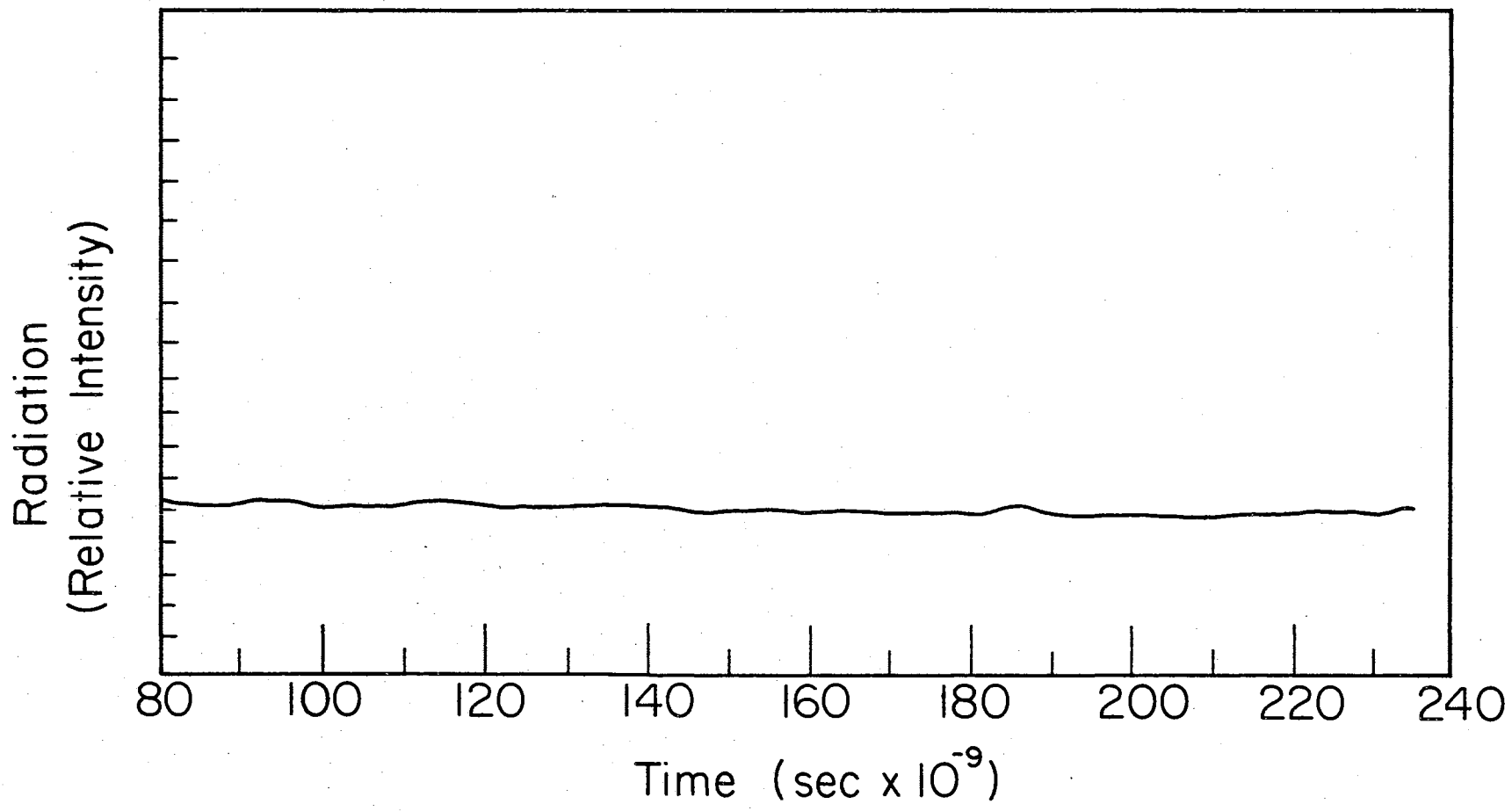Figure 21. Detected Radiation Intensity Versus Time from the Aluminum Spark Without the Scintillator in Front of the Photomultiplier's Cathode
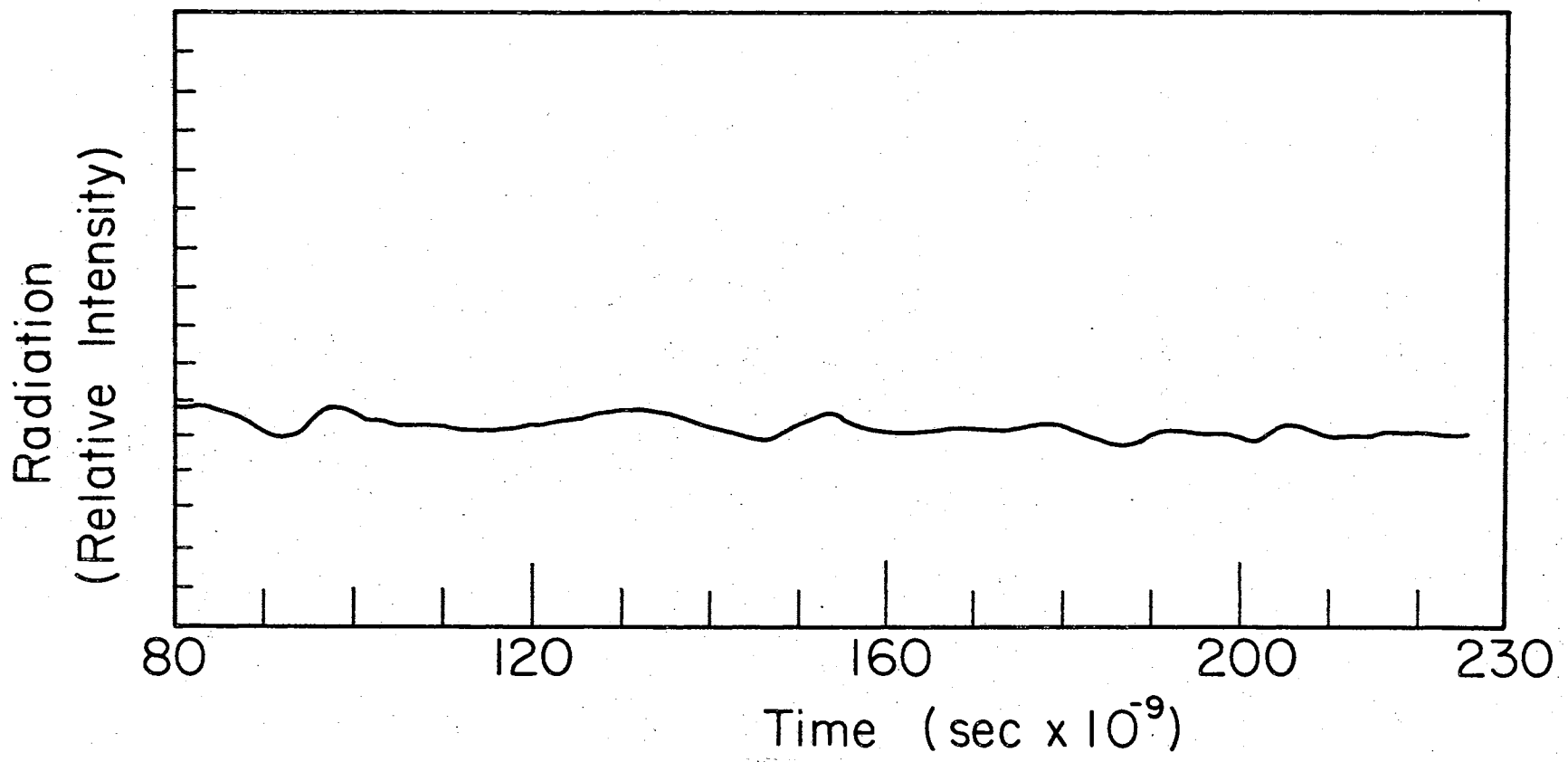
Figure 22. Detected Radiation Intensity Versus Time from the Aluminum Spark With the Scintillator in Front of the Photomultiplier's Cathode
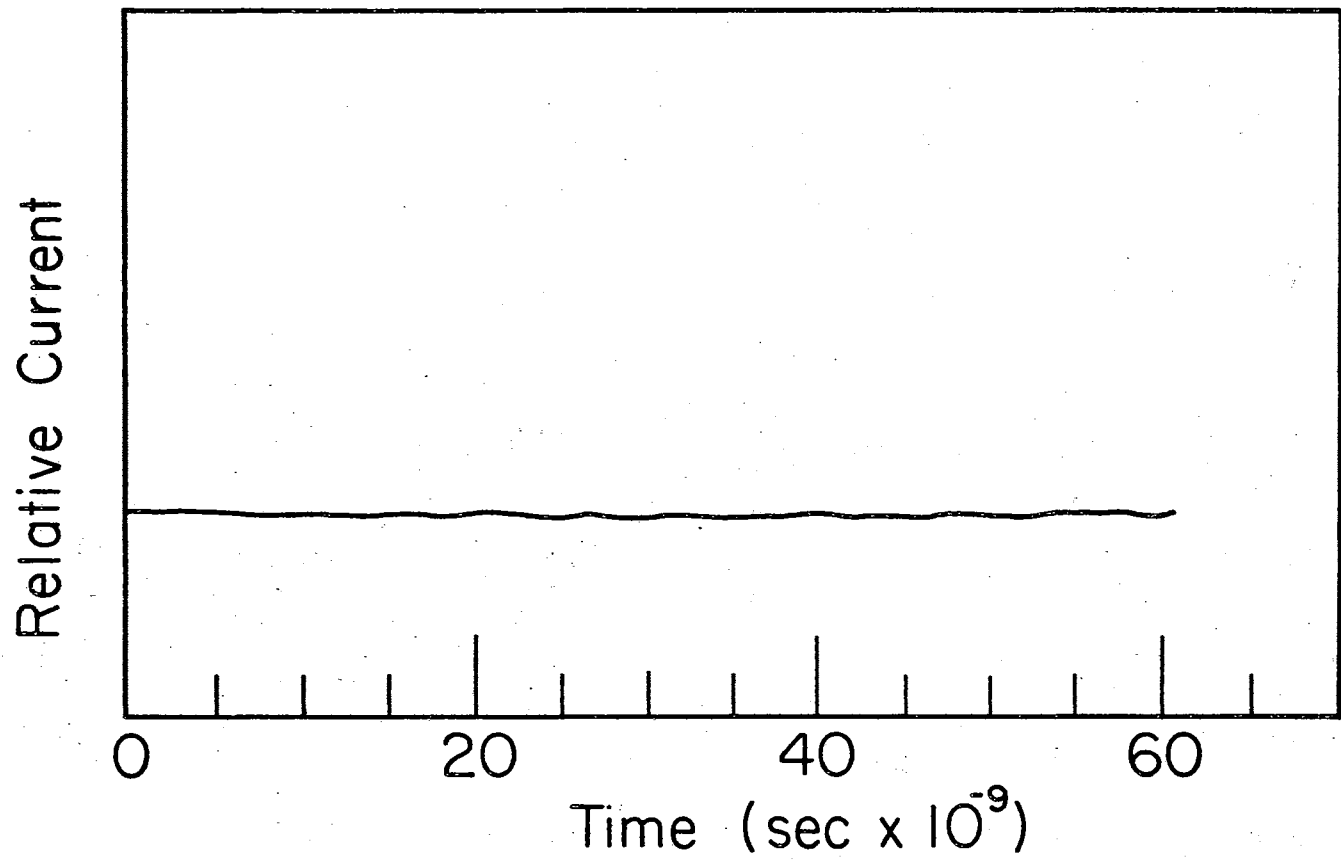
Figure 23. Aluminum Spark Current Variation with Time
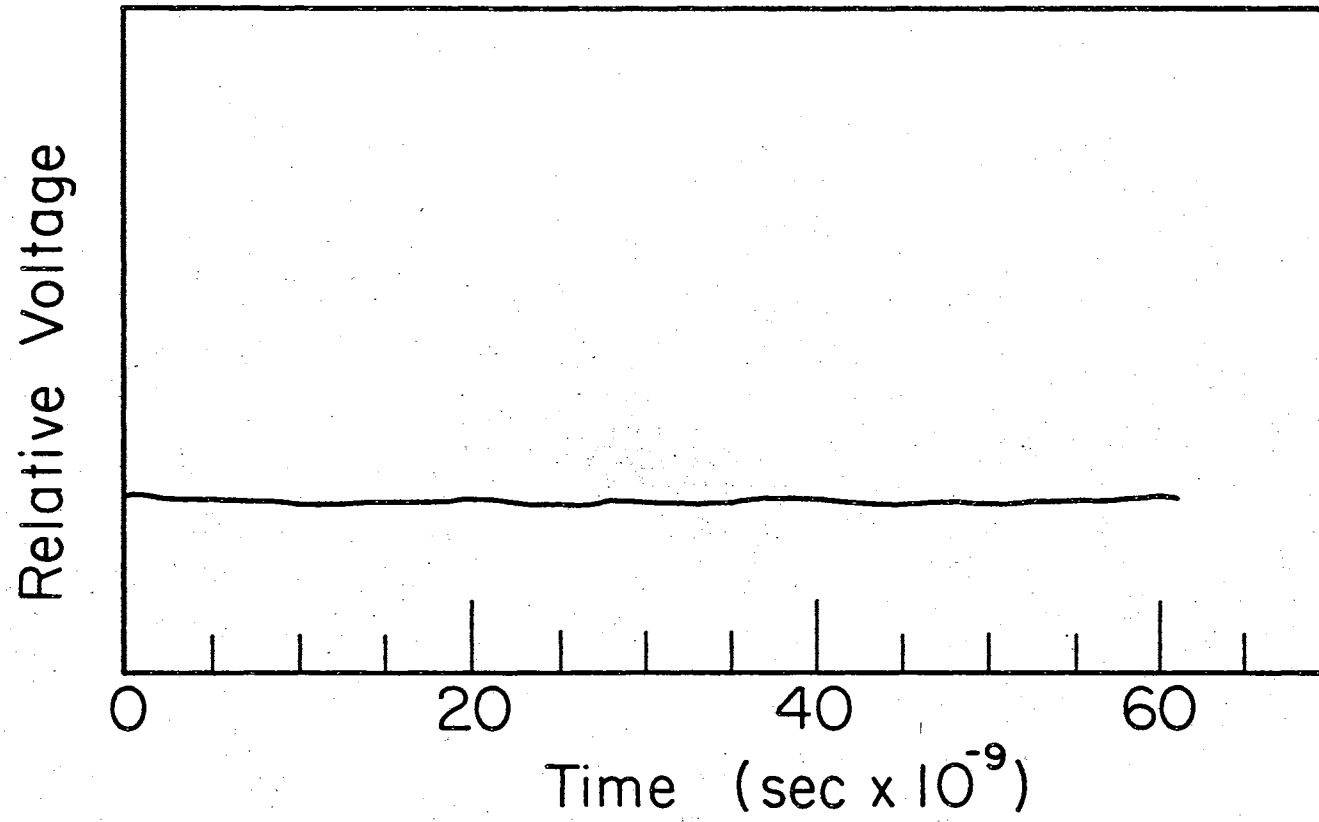
Figure 24. Aluminum Spark Voltage Variation with Time

The voltage variation with time was determined by using the circuit in Figure 25. The small capacitance was necessary in order to keep the RC time constant under a nanosecond.

For three capacitors in series

$$\frac{1}{C_t} = \frac{1}{C_1} + \frac{1}{C_2} + \frac{1}{C_3},\tag{4}$$

and if $C_1 = C_2 = C_3$, $C_t = \frac{C_1}{3}$.

Since $C_1 = C_2 = C_3 = 50\mu\mu f$, $C_t = \frac{50\mu\mu f}{3} = 16.7\mu\mu f$. $R = 51\Omega$;

$RC = 16.7 \times 10^{-12} f \times 51\Omega = .851 \times 10^{-9} sec.$

The synchronization of time with the radiation intensity graphs was accomplished by the same procedure as was described for the current monitor.

Energy Per Ion

The approximate average energy per ion was determined from 115 sparks of the aluminum spark gap. The aluminum electrodes were weighed before and after the sparking on a microgram balance. The loss in mass of the electrodes was 10.013 milligrams (total number of atoms

$$\frac{10.013 \times 10^{-3} gm}{26.9815 \ gm/at.wt} \times 6.023 \times 10^{-23} \ \frac{atoms}{at.wt} \ 2.27 \times 10^{20} atoms)$$

which represented 2.27×10^{20} atoms.

The voltage across the capacitor was recorded for each spark and the total energy was calculated by the equation $E = \frac{1}{2} CV^2$. The total energy was 3,898.4 joules. This
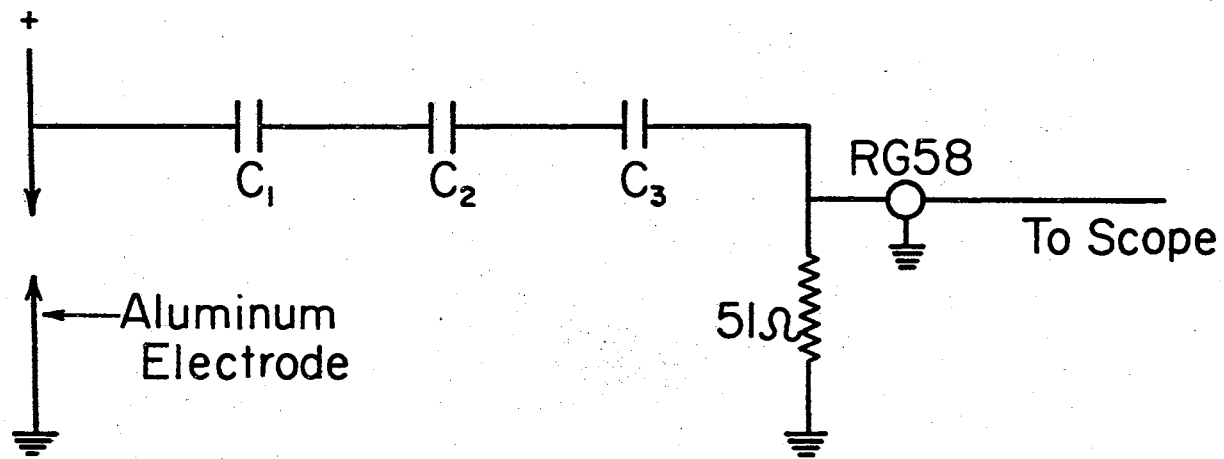
Figure 25. Schematic of the Circuit Used for the Voltage Monitor

value supplied the necessary information to complete the calculation of the average energy per ion.

$$\text{Energy per ion} = \frac{3{,}898.4 \text{ joules}}{2.27 \times 10^{20} \text{ atom} \times 1.6 \times 10^{-19} \text{ joule/ev}}$$

Energy per ion = 107.2 ev/ion

When one looks at the seven ways in which this energy is divided simultaneously in a transient plasma (thermal ionization, excitation, degeneracy density correction radiation, oscillation, and interaction,) (4) the complexity of the problem becomes more evident.

CHAPTER IV

THEORY

Introduction

Experimental progress in plasma physics is presently occurring in several areas. As an example of such progress, plasmas are employed as a controlled source of radiation for the measurement of atomic parameters such as oscillator strengths and linewidths. Several experimental programs exist which are investigating the employment of plasmas in controlled thermonuclear fusion devices. A few other examples of the different experimental and practical areas are electric arcs, electric sparks, fluorescent lamps, electrical conductivity of flames, arc welding, and arc rupture.(15) The electric spark is the area in which this author has made his investigation.

Absorption and Emission

Any study of the radiation (visible, ultraviolet, and other ranges) from a plasma involves a study of interactions between the mixture of radiation, neutral, ionized, and excited atoms which is designated a plasma. One of the most important of these interactions is the process of the absorption of energy by various mechanisms to ionize and to

48

excite atoms and ions. After their excitation, or ionization, the energy is re-emitted at the same wavelength, or at a combination of longer wavelengths.

The radiation in a plasma consists of a mixture of line radiation, a band of continuum at the end of each series and a broad continuum or bremstrahlung that is superimposed on the line radiation. Line radiation results from the transitions of electrons between permitted orbits in the atoms, or permitted orbital levels in molecules. The narrow continuum is emitted over a comparatively short range of frequencies and arises from transitions that occur near the series limit from the continuum of energy of electrons in the plasma. The broad continuum radiation, or bremstrahlung, comes from electrons in the plasma that are accelerated by the local fields or by the fields in the interior of the atoms, but that are not captured by an ion. For this reason, the origin is often said to result from a free-free transition and is designated as bremstrahlung in the foreign literature.

The bremstrahlung radiation has been shown to be small in comparison to the recombination radiation. This was proven by the condition of the film made of the aluminum-spark by a far UV spectrograph, i.e., the lines were clearly distinguishable on the film where as if the bremstrahlung radiation had been large the film would have been fogged.

Outstanding Related Theories

There are many theories that have been put forth pertaining to the characteristics of a transient plasma. The following discussion will be limited to a few of the more important theories which have provided insight as to the accepted treatment of a transient plasma.

The development of the Debye-Huckel potential is an excellent beginning place in the theory discussion. It can be developed in the following manner. Start with Poisson's equation since it is the most general expression of Coulomb's law of force between charged bodies and is written:(16)

$$\nabla^2 \Psi = - \frac{4\pi}{E} \rho \qquad (5)$$

where E = dielectric constant
 and ρ = charge density at a point.

It is so written since the distribution of charge possessing spherical symmetry depends only on the distance r of the point considered from the origin. ∇^2 is defined in polar coordinates as

$$\nabla^2 = \frac{1}{r^2} \frac{d}{dr} \left(r^2 \frac{d}{dr} \right) \qquad (6)$$

When this relation is employed, Equation 5 becomes

$$\frac{1}{r^2} \frac{d}{dr} \left(r^2 \frac{d\Psi}{dr} \right) = - \frac{4\pi}{\epsilon} \rho . \qquad (7)$$

If a particular ion is chosen as the origin of the coordinates and if no external forces are acting on the surrounding positive and negative ions, the time-average distribution of

charge about the central ion will obviously have spherical

symmetry. (16)

Denote each ion by a subscript i and a charge $Z_i e$, where

Z may be positive or negative. The condition of electrical

neutrality per unit value is satisfied by the summation

$$\sum_{i=1}^{n} Z_i e = 0$$

where n_i is the average number of ions per unit volume. The

condition of electrical neutrality further requires

$$\int_{a}^{\infty} 4\pi r^2 \rho_j \, dr = Z_j e \tag{8}$$

where $Z_j e$ is the charge on the ion that is at the origin of

the coordinate system. The limit a is the distance of

closest approach to the control ion by any other ion within

the sphere. (16)

Applying the Boltzman distribution law

$$N_i' = N_i e \left(- \frac{Z_i e \Psi_i}{kT}\right) \tag{9}$$

$Z_i e \Psi_j$ = electrical potential energy of the i-ion and N_i' is

the average local concentration of the i-ion at the point in

question.

Summing all the ionic species and recalling that the i-

ion carries a charge $Z_i e$ the charge density of ρ_j becomes:

$$\rho_j = \sum_{i} N_i Z_i e \, \exp \left(- \frac{Z_i e \Psi_i}{kT}\right) \tag{10}$$

By expanding in the form:

$$e^{-x} = 1 - x + \frac{x^2}{2!} - \frac{x^3}{3!} + \cdots$$

equation 10 becomes:

$$\rho_j = \sum N_i Z_i e - \sum N_i Z_i e \left(\frac{Z_i e \Psi_j}{kT}\right) + \sum \frac{N_i Z_i e}{2!} \left(\frac{Z_i e \Psi_j}{kT}\right)^2 \text{-------} (11)$$

By the condition of electrical neutrality $\sum N_i Z_i e = 0$, and if $Z_i e \Psi_j \ll kT$, only the term linear in Ψ is appreciable, giving the result:

$$\rho_j = -\sum_{i=1}^{s} \frac{N_i Z_i^2 e^2 \Psi_j}{kT} \tag{12}$$

The result in this approximate form is consistent with the superposition principle, since it states that Ψ is directly proportional to ρ. The approximation is only valid when the thermal energy is much greater than the potential energy. (16)

By substituting equation 12 into Poisson's equation for radial symmetry:

$$\frac{1}{r^2} \frac{d}{dr} \left(r^2 \frac{d\Psi_j}{dr}\right) = \frac{4\pi e^2}{\epsilon kT} \sum_i N_i Z_i^2 \Psi_j \tag{13}$$

Let $K^2 = \dfrac{4\pi e^2 \sum\limits_i N_i Z_i^2}{\epsilon kT}$ and substitute into equation 13. (14)

$$\frac{1}{r^2} \frac{d}{dr}\left(r^2 \frac{d\Psi_j}{dr}\right) = K^2 \Psi_j \tag{15}$$

Choose $U = \Psi_j r$ and equation 15 reduces to:

$$\frac{d^2 U}{dr^2} = K^2 U \tag{16}$$

which has the general solution:

$$U = Ae^{-Kr} + Be^{Kr} \tag{17}$$

or

$$\Psi_j = A \frac{e^{-Kr}}{r} + B \frac{e^{Kr}}{r} \tag{18}$$

where **A** and **B** are constants of integration. Since the potential must remain finite at great values of r it is necessary that B = 0.

Equation 18 now becomes:

$$\Psi_j = A \frac{e^{-Kr}}{r} \tag{19}$$

which is also known as the Yahawa potential. $\frac{1}{K}$ has dimensions of length and is called the Debye length.

The Debye length is a minimum length for macroscopic charge separation effect in a plasma and a minimum length for individual Coulomb effect, (1) i.e., the potential at distances greater than $\frac{1}{K}$ from a given charge is dropped. This cut-off point is quite reasonable when one considers the effect of the overlap for a large number of particles, i.e., the potential would become infinite.

A can be evaluated by substitution Ψ_j in equation 12:

$$\rho_j = -A \frac{e^{-Kr}}{r} \sum_i \frac{N_i Z_i^2 e^2}{kT} = -A \frac{K^2}{4} \cdot \frac{e^{-Kr}}{r} \tag{20}$$

By substituting for ρ_j in equation 8 equation 20 becomes:

$$Ak^2 \epsilon \int_a^\infty re^{-Kr} \, dr = Z_i e. \tag{21}$$

Integrating equation 21 by parts one obtains:

$$A = \frac{Z_j e}{\epsilon} \cdot \frac{e^{Ka}}{1+Ka} .$$

The Debye-Huckel potential can now be expressed as:

$$\Psi_j = \frac{Z_i e}{\epsilon} \cdot \frac{e^{Ka}}{1+Ka} \cdot \frac{e^{-Kr}}{r} . \tag{22}$$

Two more important questions to be answered pertaining to a plasma are: (1) What is the population of levels within the given species? (2) What is the relative total populations of successive ionization states?

The answer to the first question is given in mathematical form by Maxwell-Boltzmann statistics in the following manner. The population density of state p of the species S_z, $N_z(P)$ is thus:

$$\frac{N_z(P)}{N_z} = \frac{g_z(P)}{B_z(T_e)} \exp \left(- \frac{E_z(P)}{kT_e}\right) \tag{23}$$

where T_e is the electron temperature, $g_z(P)$ is the statistical weight of the Pth state measured from its ground state (i.e. $E_z(1) = 0$), N_z is the total number density of S_z and $B_z(T_e)$ is that part of the appropriate ionic partition function due to excitation. (17)

$$B_z(T_e) = \sum_P g_z(P) \exp \left(- \frac{E_z(P)}{kT_e}\right) \tag{24}$$

The answer to the second question was given in mathematical form by Saha. Saha's equation is developed in the following manner by (J. Cooper), for a system when local thermodynamic equilibrium is assumed.

Consider a plasma consisting of neutral atoms, ions of charge 1 to Z, and electrons. Let their number densities be n_0, n_1, ..., n_z, n_e respectively, and their total numbers be N_0, N_1, ..., N_z, N_e.

The Helmholtz free energy F is given by

$$F = - kT \ln Q \tag{25}$$

where Q is the partition function of the whole system and in the limit of no interactions between the particles of the plasma (when F is equal to F_0)

this equals the product of the partition functions of the individual species.

$$Q = Q_e \prod_{Z=0}^{Z} Q_z \tag{26}$$

with

$$Q_e = \frac{(U_e)^{N_e}}{N_e!} = \frac{1}{N_e!} \left[2V \left(\frac{2\pi mkT}{h^2}\right)^{3/2} \right]^{N_e} \tag{27}$$

$$Q_z = \frac{(U_z)^{N_z}}{N_z!} \tag{28}$$

where U_e and U_z are partition functions of an individual electron and an individual ion respectively. U_e is purely translational, while $U_z = T_z B_z$ where T_z is the translational and B_z the internal or excitational part of the ionic partition function. For the reaction

$$S_{z-1} = S_z + e$$

conservation of charge gives

$$-\delta N_{z-1} = \delta N_z = \delta N_e \tag{29}$$

and for equilibrium

$$\delta F = \frac{\partial F}{\partial N_{z-1}} \delta N_{z-1} + \frac{\partial F}{\partial N_z} \delta N_z + \frac{\partial F}{\partial N_e} \delta N_e + \frac{\partial F}{\partial P} \delta P = 0. \tag{30}$$

As F does not contain the pressure P explicitly the condition for equilibrium becomes

$$\frac{\partial F}{\partial N_e} - \frac{\partial F}{\partial N_{z-1}} + \frac{\partial F}{\partial N_z} = 0. \tag{31}$$

Using Stirling's formula ($\log n! = n \log n - n$ for n large)

$$\frac{N_z N_e}{N_{z-1}} = \frac{U_e U_z}{U_{z-1}} \tag{32}$$

where the one-particle partition functions U are reckoned from the same energy zero.

$B_z(T_e)$ and $B_{z-1}(T_e)$ are written as the internal partition functions for the species S_z and S_{z-1} with their energy levels referred to the respective ground states of the individual species.

Then

$$\frac{n_z \, n_e}{n_{z-1}} = 2 \left(\frac{2\pi m k T_e}{h^2}\right)^{3/2} \frac{B_z(T_e)}{B_{z-1}(T_e)} \exp\left[-\frac{E_{z-1}(\infty)}{kT_e}\right] \begin{matrix}(\text{Saha's} \\ \text{equation})\end{matrix} \quad (33)$$

where $E_{z-1}(\infty)$ is the ionization energy of the
species S_{z-1}^1. This equation, which gives the ratio
at equilibrium of the total population densities of
the ionic species S_z to that of S_{z-1}, is known as
Saha's equation. Consequently, the composition of
a plasma with ions up to charge Z is described by Z
Saha equations and the equation of charge neutrality

$$n_e = \sum_{z=0}^{z} Z n_z . \,(17) \qquad\qquad (34)$$

Fundamental Postulates and Discussion of Data

Equilibrium, Temperature and the Conservation of Energy

During the period of current conduction by a spark in

the vacuum, a dense plasma (a mixture of electrons, ions and

atoms) is emitted from a small area on an electrode. This

area is in the immediate vicinity of a pointed tip, or of a

small insulating particle, according to the survey of pub-

lished information that is presented in the introduction to

this thesis. Since the spark channel and the area of intro-

duction of the plasma into vacuum is small, the initial

density and the initial temperature are both high. These

are the conditions for the rapid establishment of equilib-

rium. Lengthy estimates indicate that initial equilibrium

exists in the experiments that are presented in this thesis.

Provided equilibrium exists between the modes of energy

storage by the electrons, the atoms, and the ions, the qual-

itative interpretation in this section is possible.

For electrons, the energy is only stored in the form of kinetic energy. For ions and atoms, the energy may be in the form of kinetic energy, in the degree of ionization, in excited states, and so forth. Energy is also in the plasma in the form of radiation which is in equilibrium with the excited states. The relative amount of energy in each of these modes is a function of the total energy, the volume, and the density of the plasma. The distribution of energy between modes is described and calculated in the thesis by Bruce.(4) Equilibrium requires that each of these modes for the storage of energy should be filled according to the Boltzmann relation,

$$\tfrac{1}{2}m_e v^2 = \tfrac{3}{2}kT, \tag{35}$$

where m_e and v are the mass and the <u>random</u> velocity of the electrons, k is Boltzmann's constant, and T is the temperature. For this relation to apply to the electrons in a plasma, the velocity, v, must be the random velocity. This means that the vector sum of all of the velocities of all electrons in unit volume satisfies the relation

$$\sum_{i=1}^{N} \vec{v_i} = 0. \tag{36}$$

The velocity, v_i, is for the i th electron and the summation is over all electrons, N, in unit volume. Unit volume must be sufficiently large for N to be a very large number.

An explanation of the expansion with time of a dense plasma in a vacuum is simplified by selecting a simple

initial shape for the plasma. In the thesis by Bruce, the
initial shape of the dense plasma is assumed to be a sphere.
At zero time, the plasma in the sphere is assumed to be in
equilibrium as well as at constant temperature, and the veloc-
ities of the particles satisfy equation 36. As time progres-
ses, the plasma expands into the vacuum. During the expansion,
several factors influence the distribution of the energy be-
tween the storage modes for the energy and these affect the
total kinetic energy of the electrons. (4) These factors are
too lengthy to discuss at this time. The attention at this
time is focused entirely on the distribution of the kinetic
energy of the electrons between a radial component of the ve-
locity and a random component. The random component of the
velocity determines the temperature and must satisfy an equa-
tion of the form in equation 36. In vector form the total
velocity $v(r,t)_i$ of the i th electron divides into two
components

$$v(r,t)_i = v(r,t)_i(\text{random}) + v(r,t)_i(\text{radial}). \qquad (37)$$

All of these quantities are a function of the radius of the
sphere and the time since the expansion started.

As the expansion proceeds in its early stages, the radial
component of the velocity increases with respect to the ran-
dom component of the velocity. Other considerations show
that the fraction of the total energy which is kinetic energy
of the electrons increases as the temperature falls. Even
with this change, the increase in the radial component of the
velocity with respect to the random component results in the

formation of a cold, rarified outer to relative dense shell on the expanding sphere. The increase of v(radial) with the radius also quickly affects the radial distribution of the density. In a very short time the initially uniform expanding sphere transforms very rapidly into a sphere with a rarified, to dense cold, outer shell about an intermediately dense hot, inner core.

Methods for Obtaining and Presenting the Results

The basic definitions and postulates in the preceding paragraphs are necessary as a background to the explanation of the results that were obtained. The results show the emission of light from a spark immediately after the breakdown of the gap between spectroscopically pure aluminum electrodes in a vacuum. The emitted light is assumed to be a sampling method for ascertaining the physical phenomena, in particular the temperature, of the expanding plasma. It is necessary to assume that the emitted radiation does not have sufficient intensity (power drain from the plasma) to affect the equilibrium that is postulated for the expanding plasma. Before proceeding with a discussion of the data, the physical system for measuring the light, the starting time for the oscilloscope, and the order of presentation of the measurements are presented.

The emitted light from the spark is measured in two ways. In the first set of experiments, the spark is viewed directly by an RCA 6199 photomultiplier tube with both the spark gap and the tube in a single, evacuated chamber. In

the second series of tests, a scintillator in the form of a
thin sheet of plastic is placed on the glass face of the
photomultiplier tube between the spark and the tube. This
scintillator absorbs all light with a wavelength of less
than 3800 Å, and transmits 89.4 per cent of the light in the
visible. The scintillator is excited to emit radiation in
the visible by the incidence of photons in the ultraviolet.
The ultraviolet is incident on the side of the scintillator
that is opposite to the glass face of the photomultiplier
tube so only fluorescent radiation with wavelengths longer
than about 3900 Å are transmitted to the photomultiplier.
The scintillator has a decay time of 2.9 nanoseconds.(14)
Since fluorescent radiation is emitted in all directions, as
from most sources, geometric considerations show that less
than half of the emitted fluorescent radiation can reach the
cathode of the photomultiplier tube. In addition, a sub-
stantial fraction of the fluorescent light has a shorter
wavelength than 3800 Å. Since this light is emitted on the
side of the scintillator that is opposite to the photomulti-
plier tube, this part of the emitted radiation cannot pene-
trate the scintillator.

The oscillograph is triggered by the circuit that
pulses the photomultiplier tube. The trigger is timed to
start the sweep on the oscillograph after electrical conduc-
tion is established through the spark gap. This is an
important consideration, for it avoids the rapid variation
of the current and voltage as the breakdown occurs but still

starts the recording sweeps within one to three nanoseconds after the completion of the breakdown. The short time delay is known from the variation of the intensity after the recording starts. After the recording of the oscillograph sweep starts, it requires about $8\frac{1}{2}$ nanoseconds for the intensity to reach a maximum. The time to reach a maximum is approximately the half-life of the excited states in the atom. This time is known from the uncertainty principle which establishes that the energy in the excited state cannot be known exactly. The rule of thumb for the half-life time for the emission of a spectral line is of the order of 10^{-8} seconds, or 10 nanoseconds. From a comparison between this time and the measured time to reach a maximum, the breakdown time is perhaps one to three nanoseconds before the sweep starts.

Discussion of the Results

The new information from the results of this research project is derived from the explanation of the oscillations in the visible light that is emitted and in the tendency for this oscillation to be absent when the scintillator is in the light path. The "damped" oscillation in the visible light starts immediately after electrical conduction is established through the spark gap and is damped within approximately 60 nanoseconds.

The presented results are confined to the time period from one to three nanoseconds after breakdown of the gap until approximately 230 nanoseconds after breakdown. During

this period, the power input to the spark channel does not vary with time. This is shown by the substantially constant current for the first 60 nanoseconds which was recorded by the oscilloscope. This is presented in Figure 23. A similar trace for the voltage over the same time interval is shown in Figure 24. The power input to the spark is constant over this initial short period of 0.06 microseconds but the power input would be a variable on a much longer time scale. The L-C circuit, with a condenser as a source of power, is actually an oscillatory circuit with a period of the order of a millisecond.

After the initial fluctuations in the light intensity, the emitted light intensity gradually decreases with a fair amount of steadiness. The emitted light for the period from 80 to 230 nanoseconds is recorded in Figure 22 when the scintillation film is in position. The emitted radiation during the same period is presented in Figure 21 for the scintillator removed from the optical path. There is only a slight difference between the two figures. The signal with the scintillator is slightly higher and perhaps shows more fluctuations.

With the scintillation film in position, the intensity of the emitted light for the time interval from 40 to 80 nanoseconds is shown in Figure 20. The light fluctuations without the scintillator for the same time interval is shown in Figure 19. Both figures show some oscillation

with a tendency toward regular periods. The average light emission is not significantly different in Figures 19 and 20.

With the scintillator in position, the intensity of the emitted light for the time interval from 0 to 40 nanoseconds is presented in Figures 16 and 18. The two traces show the reproducibility of the radiation from two entirely different sparks. The electrode positions were even adjusted between these sparks. There is not much oscillation in the recorded intensity. The light fluctuation without the scintillator and for the same time interval are presented by the curves in Figures 15 and 17, which are for different sparks. The results are all typical of the many measurements that were made. If some of the smaller fluctuations in intensity are ignored, the average intensity with the scintillator in position is a little higher, rises to the first peak a little more rapidly and has very little oscillation in the intens- ity. The large oscillations in the intensity are observed when the scintillator is not employed.

The most obvious characteristic of the intensities that are shown in the curves from Figures 15 to 18 is the initial low intensity and the rise in this intensity to a maximum value. The exact position of the peak may be influenced by the breakdown mechanism, but the general features of this rise are to be expected from the uncertainty principle. The uncertainty in time and energy cannot be less than $\Delta E \Delta t = h$. As a consequence of this uncertainty, the mean lifetime of the excited states is generally stated in textbooks on

atomic spectra to be about 10^{-8} seconds, or 10 nanoseconds. For the curves in Figures 15 and 17 which do not have the scintillator, the time from the start of the sweep until the peak is about $8\frac{1}{2}$ nanoseconds. As mentioned previously, there may be an uncertainty of 1 to 3 nanoseconds in the time at which the measurement of the rise time should be started.

Confirmation for attributing the initial rise time to this phenomena comes from the slightly more rapid rise time when the scintillator is in position. There is no difference in the average spark, so the difference must be sought in the scintillator which is the only thing that has been changed. The scintillator may do two things: detect an earlier peak in the intensity of the ultraviolet which is unlikely, or more probably increase the rate of rise from the decay time of 2.9 nanoseconds for excited states in the scintillator. The latter assumption means that excited states in the scintillator which result from the absorption of radiation begin to contribute to the intensity about 3 nanoseconds later. This means that the peak of radiation that is absorbed in the first 4 nanoseconds of the sweep would be emitted about 7 nanoseconds after the start of the sweep.

Interpretation of Data

The assumption was made, at the start of this section, that equilibrium existed between the modes of energy storage

when the plasma was ejected from the anode. The initial increase in intensity is in agreement with this assumption although it does not necessarily prove that it existed initially. This is, however, the simplest assumption. The initial increase in intensity of the visible radiation (no scintillator) and of the visible radiation plus the ultraviolet (scintillator in position) is in agreement with this assumption of equilibrium.

In the introduction and in the early part of this section, a mechanism for breakdown was proposed. This proposal was based on the analytical work of Bruce for his thesis and on publications that were cited. The proposed mechanism postulated the ejection of a dense jet of electrons, excited atoms, and ions in the form of a plasma from the anode. Energy equilibrium is assumed to exist between all modes of energy storage among these particles. The measurements on the rise in intensity are in semi-quantitative agreement with this concept. The jet expands into the vacuum in the form of a hemisphere and this fact is established by published photographs.

The analytical studies of Bruce give the basis for the observed variation of the intensity. The profiles of different variables were calculated and plotted as a function of the radius of the sphere at different instants of time during the expansion. The initial assumptions by Bruce are slightly different from the conditions in this problem but the results are equivalent, so far as the light emission is

concerned. Bruce assumed that each atom in a solid sphere
is suddenly given a considerable energy. This energy is
divided between all modes of energy storage and they are
assumed to come to equilibrium. In the expansion of the
sphere that follows this initial equilibrium, the density
and the pressure profiles are shown at 2.744 nanoseconds
after the expansion starts in Figure 26. The temperature
and ionization at the same time are shown in Figure 27.
After the expansion has proceeded for 10.74 nanoseconds, the
density and pressure profiles are shown in Figure 28. The
corresponding temperature and ionization are shown in Fig-
ure 29.(4)

As the expansion proceeds, a relatively dense and slow
moving, cold shell forms about the lower density, very hot
interior of the sphere. This condition is intrinsically
unstable. From photographs of exploding wires, the shell is
known to break up and permit jets of the hot interior to
come through the breaks. The jets are quickly cooled and a
second cold, but irregularly shaped, cold shell is again
formed. This break-up of the cold shell and its reconstitu-
tion may occur several times as the temperature of the hot
core cools.

From this rough outline of the behavior of an expand-
ing plasma, the anticipated light emission from the spark
may be predicted. The outer portion of the ejected jet
tends to expand in the form of a hemisphere. The outer
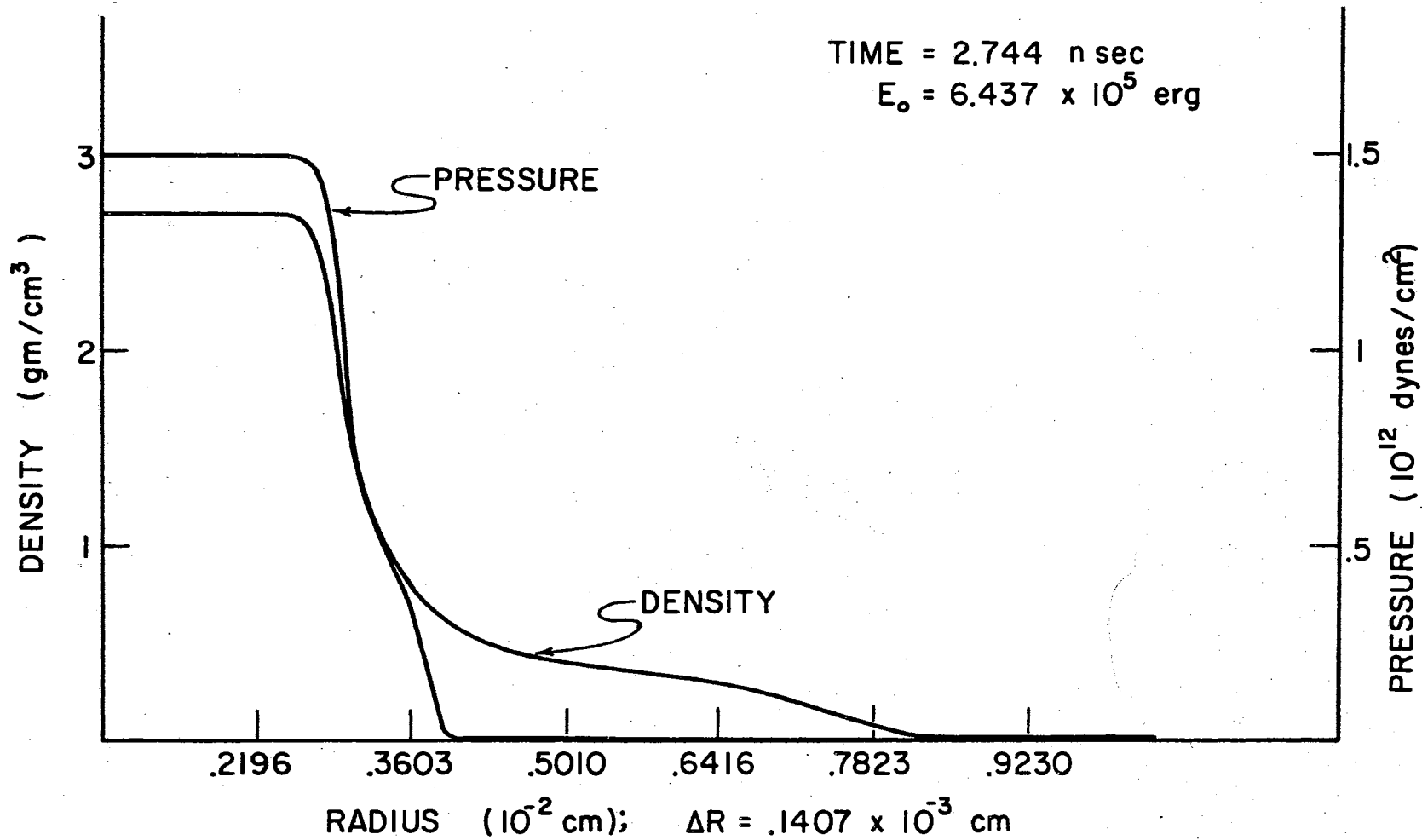shell of this hemisphere forms a cold, partially opaque,

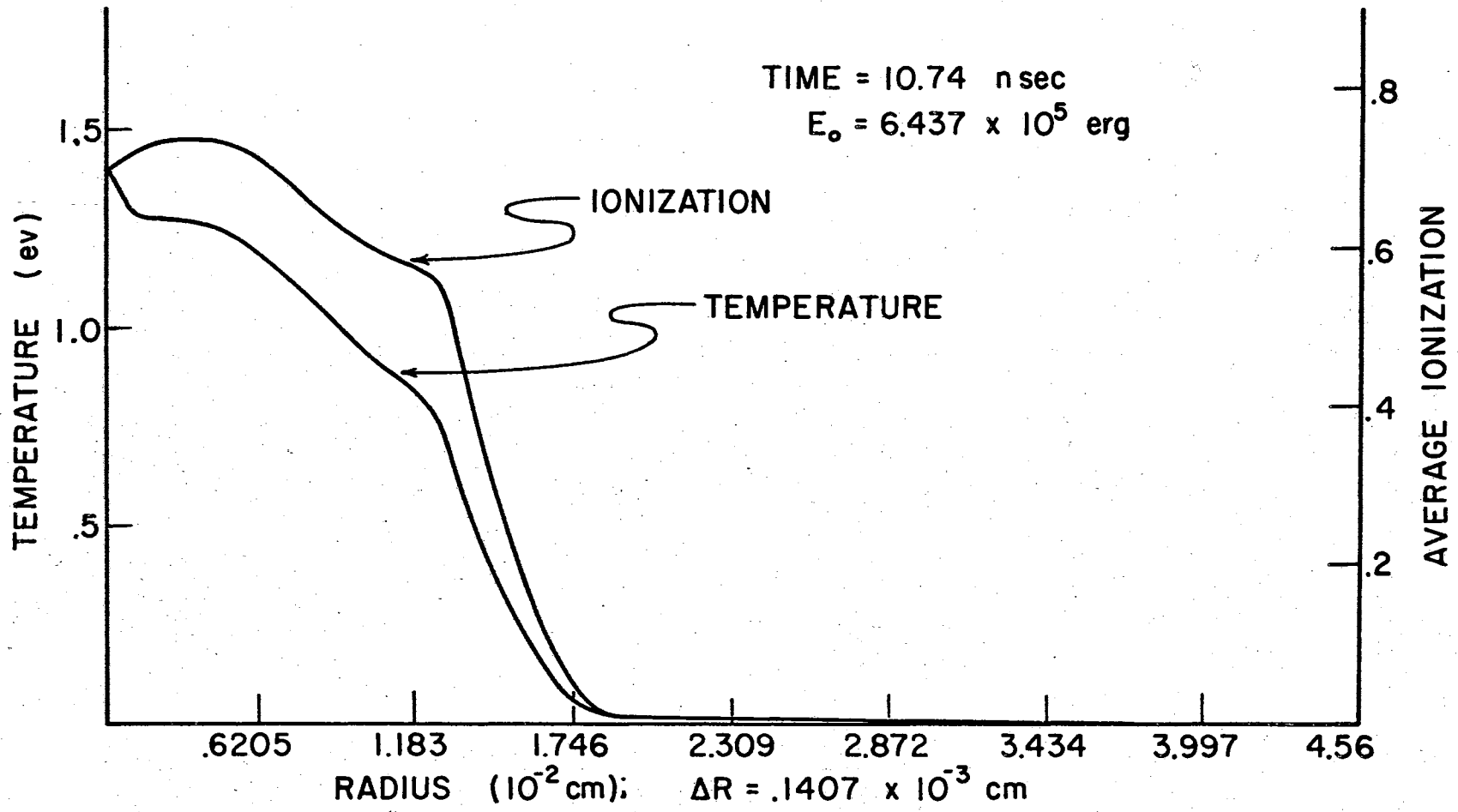Figure 26. Density and Pressure Versus Radius from Bruce's Thesis

Figure 27. Temperature and Average Ionization Versus Radius from Bruce's Thesis
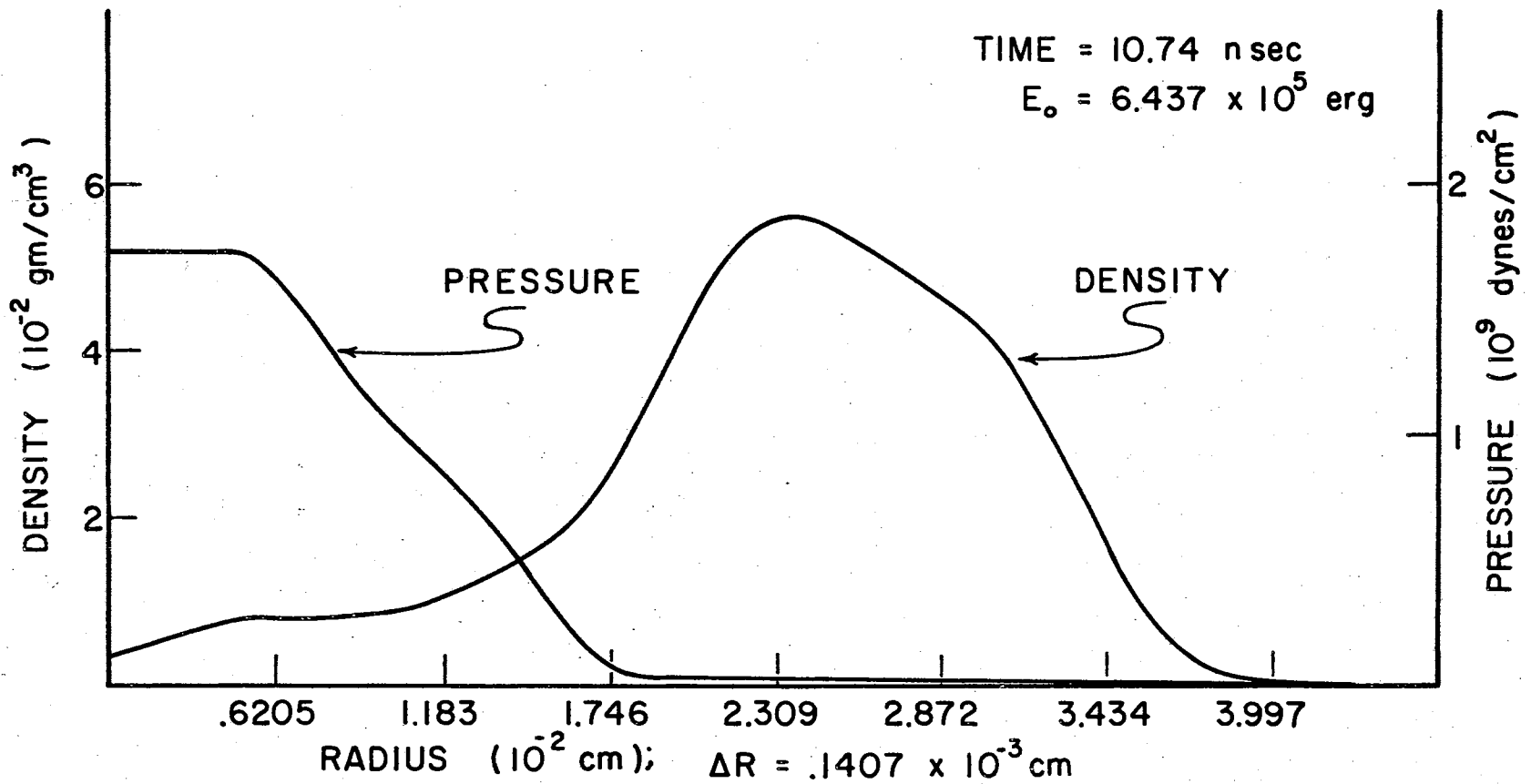
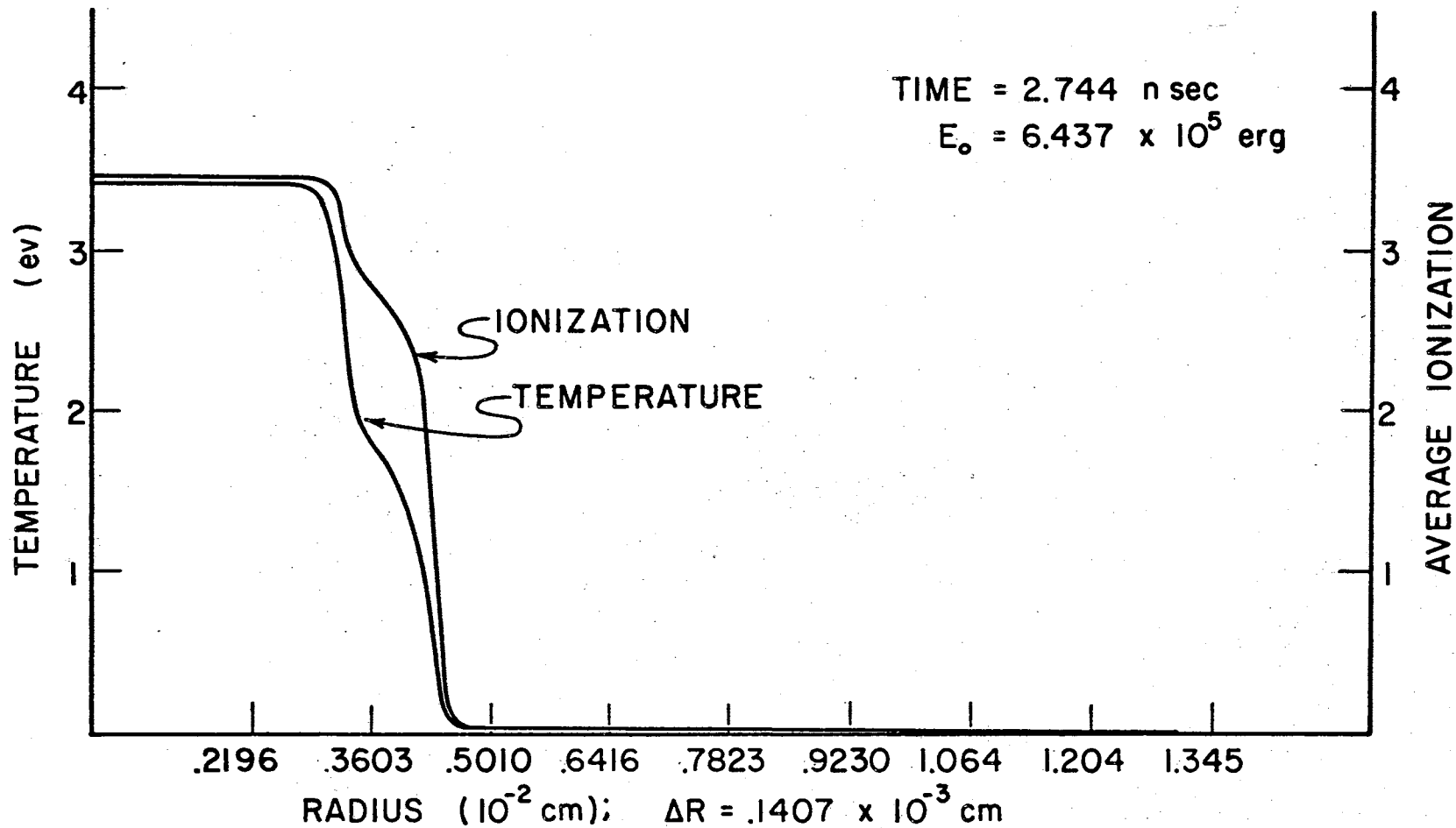Figure 28. Density and Pressure Versus Radius from Bruce's Thesis

Figure 29. Temperature and Average Ionization Versus Radius from Bruce's Thesis

shell. This shell emits less and less light and that light intensity must correspond to the cold temperature of the shell since it prevents the high temperature radiation from escaping from the core. Compare these predictions with the observed intensity variations for the spark that are shown in Figures 15 to 19. The initial rise in the radiation has been discussed. The peak in the emitted radiation corresponds to the initial temperature, as a consequence of the half-life of the excited atom before emission of the radiation. The subsequent decrease in the <u>visible</u> radiation is a consequence of two phenomena: (1) the formation of a cold, increasingly opaque shell which intercepts the radiation from the hot core, and (2) the lower temperature of the cold shell which (a) lowers the intensity and (b) fails to replace the low energy, excited states which have radiated during the first peak of the radiation. The subsequent rise in intensity corresponds to the increase in intensity when the cold shell breaks and exposes the hot core. Observe that the second rise in intensity is a little more rapid than the mean time for the first rise. The break up of the shell is more rapid than the half-life of 10 nanoseconds for the excited atoms. The core is radiating continuously at an intensity that corresponds to its temperature. (18)

For the preceding explanation to be accepted, the general change in the shape of the intensity-time curve must be explained when the scintillator is in position in the light beam. The average change requires a large pulse of

ultraviolet in the time period from 10 to 18 nanoseconds after the start of the sweep. There is a 2.9 nanosecond delay in the scintillator which shifts the recorded peak to 13 to 21 nanoseconds. Another secondary pulse of ultraviolet should follow in the 25 to 35 nanosecond interval. Consider the origin of the ultraviolet during the period from 12 to 22 nanoseconds. A minor source may be the far-ultraviolet radiation that penetrates the thin outer shell. Estimates show that some radiation probably comes from this source. A more probable source of the ultraviolet radiation is from the direct emission of ultraviolet from the cold shell. During the peak in the emission of the far-ultraviolet, a substantial portion of this radiation is re-absorbed to excite atoms that are forming the cold shell, and these must re-emit the radiation about 8 to 10 nanoseconds later, or 13 nanoseconds later as observed by the photo-multiplier tube with the scintillator in position. Radiation absorbed from the initially excited atoms would be absorbed to excite atoms in the period from 3 to 11 nanoseconds and would be re-emitted in the period from perhaps 13 to 21 nanoseconds.

The second pulse of radiation in the ultraviolet would originate in the same manner during the second peak of visible radiation plus its accompanying ultraviolet emission.

CHAPTER V

FUTURE EXPERIMENTS

The Laser

There are many experiments, which can be conducted with a pulsed photomultiplier, and each year new explorations are being initiated. Such studies are presently being done in Dr. Todd's research laboratory at Oklahoma State University. Four future experiments which may provide interesting and enriching in the field of plasma physics will be mentioned in this presentation. They include the use of an exploding wire, the use of a ruby laser to produce transient aluminum plasmas, the improved gain factor, and the line measurements inside the ultraviolet spectrograph.

The first study of consequence is the high energy pulsed ruby laser. This can be used to produce aluminum plasmas by the impengment of a giant laser pulse on an aluminum target positioned in a vacuum chamber. The high intensity laser pulse should last approximately 50 nanoseconds according to Lengyel.(19) The 130 nanosecond pulse applied across the photomultiplier's dynode resistors should be satisfactory for viewing the plasma produced by the laser pulse impact on the aluminum target.

The triggering of the pulsing generator can be accomplished in a similar manner as was used for the aluminum spark. The detecting phototube can be positioned in the path of the radiation emitted by the flash tubes that trigger the laser.

The pulsed photomultiplier will be placed in a vacuum chamber a few centimeters from the aluminum target. The output from the photomultiplier which is a measurement of the emitted radiation intensity versus time from the aluminum plasma will be recorded by the same procedure as the one used for the aluminum spark.

The Exploding Wire

A procedure by which an aluminum wire can be exploded is also currently being considered. Plans include using pulse voltages up to 100 KV and one microsecond in length in order to explode the wire. This will then produce a transient plasma whose emitted radiation can be investigated by the pulsed photomultiplier. The design is such that the vacuum chamber in which the photomultiplier is currently housed will connect onto the vacuum chamber which will serve as the explosion chamber for the aluminum wire.

Triggering the pulsing generator is the next concern. The 100 KV pulse will traverse 1700 ft. of coaxial cable before exploding the wire. The pulse generator that activates the P.M. can be triggered by tapping off the coaxial cable with a tee connector and bridge. The pulse obtained

at the tee can then be applied across the control grid of
the first 2D21 thryatron in the pulsing generator so that
the photomultiplier is pulsed at the instant the wire
explodes.

Improved Gain Factor

A third research endeavor concerns an improved gain
factor. An improvement in the gain factor of the intensity
versus time measuring device can be accomplished by at least
two methods: either increasing the pulse voltage or combin-
ing an electron multiplier with the photomultiplier that is
presently in use and pulsing both with a high voltage square
pulse simultaneously.

The first method has an advantage in that it would be
much simpler to put into operation. A strong disadvantage
would be the limitation placed on the magnitude of the pulse
voltage across the dynode resistors in order to prevent
arcing.

The second method seems the more desirable in insuring
a large increase in the gain factor. It requires the use of
two similar pulsing generators. The cathode of the electron
multiplier will be positioned in the path of the far ultra-
violet radiation emitted by the plasma. At the approximate
time the radiation strikes the cathode the electron multi-
plier will be pulsed with 5 KV. The output from the
electron multiplier will then traverse a 10 KV potential and
strike a scintillation screen placed in front of the

photomultiplier's cathode. The pulsed photomultiplier then amplifies the signal it receives from the scintillator and feeds it into an oscilloscope where it can be photographed.

Line Measurements Inside Ultraviolet Spectrograph

A fourth study being conducted concerns line measurements inside an ultraviolet spectrograph. A far-ultraviolet spectrograph (100 to 1200 $\overset{\circ}{A}$) has been built by Payne and calibrated by Carpenter. The equipment which was presented in Section III of this chapter could be used to measure the relative intensity of the aluminum lines (from 100 to 1200 $\overset{\circ}{A}$) for the four methods that are available or will soon be available in Todd's laboratory to produce aluminum plasmas. These methods include use of the aluminum spark, laser, exploding wire, and hyper-velocity impact.

The electron multiplier and the photomultiplier can be located inside of the spectrograph. The electron multiplier's cathode will be positioned at the focusing point of the line under investigation. By using the matched impedance vacuum feedthroughs described in Chapter two the high voltage pulses can be transmitted into the spectrograph to the electron multiplier and photomultiplier and the output from the photomultiplier back out to the oscilloscope and camera.
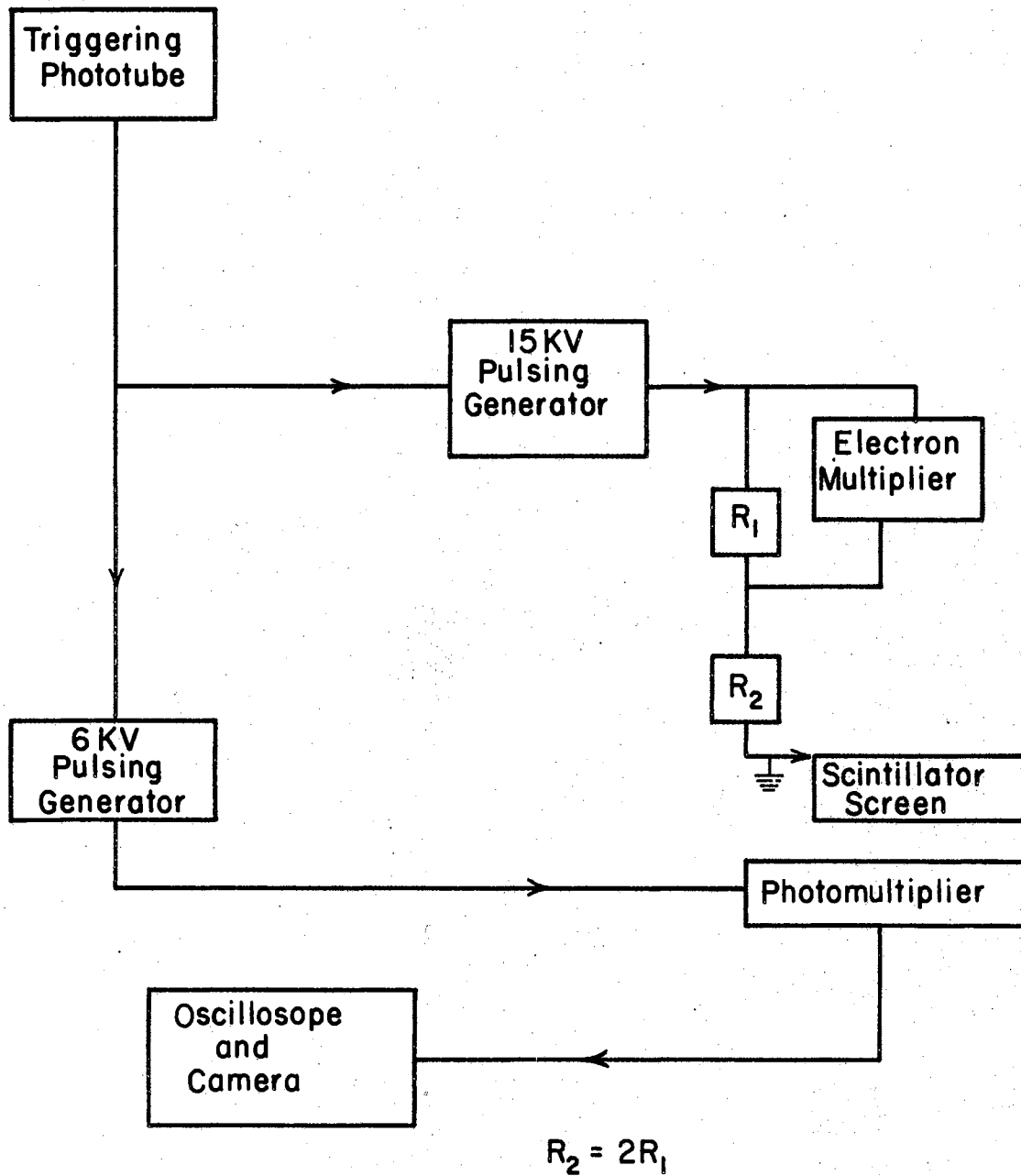
Figure 30. Block Diagram for Proposed Line Intensity Versus Time
Measurement

BIBLIOGRAPHY

(1) Shkarofsky, I. P., T. W. Johnston, and M. P. Bachynski. The Particle Kinetics of Plasmas. Reading, Massachusetts: Addison-Wesley Publishing Company, Inc., 1966.

(2) Compton, K. T., and Irving Langmuir. "Electrical Discharges in Gasses." Review of Modern Physics, II (April, 1930), 123.

(3) Kittel, Charles. Introduction to Solid State Physics. 3rd ed. New York: John Wiley and Sons, Inc., 1966.

(4) Bruce, Rufus E. A Model and Calculations for the Properties of an Exploding Plasma Sphere. Unpublished Doctoral Dissertation. Stillwater, Oklahoma: The Oklahoma State University, 1966.

(5) Meek, J. M., and J. D. Craggs. Electrical Breakdown of Gases. Oxford, England: Clarendon Press, 1953.

(6) Cobine, J. D. Gaseous Conductors. New York: Dover Publications, Inc., 1958.

(7) Wahr, J. C., W. W. McCormick, and R. A. Sawyer. "Emission Characteristics of Vacuum Spark Discharges." Journal of the Optical Society of America, XLIII (March, 1953), 153-156.

(8) Post, R. F. "Performance of Pulsed Photomultipliers." Nucleonics, X (May, 1952), 46-50.

(9) Singer, Sidney. Measurement of Rise and Decay Times of Three Fast Scintillators Including a Special Plastic. Los Alamos, New Mexico: Los Alamos Scientific Laboratory, LA-1694, (September, 1953).

(10) Radio Corporation of America. Phototubes and Photocells Technical Manual: PT-60. Lancaster, Pennsylvania: Radio Corporation of America, 1963.

(11) Slater, R. R., and F. C. Todd. Analytical and Experimental Study of the Mechanisms of Penetration and Light Emission for Micrometeoroids Impact on an Aluminum-Coated Photomultiplier. Quarterly Progress Report No. 9, Contract NASr-7, (December, 1962).

(12) Detweiler, H. D., and D. E. Solomon. "Microwave
        Frequency Feed-through for Vacuum System," The
        Review of Scientific Instruments, XXXVII (January,
        1966), 126.

(13) Wald, Alvin. "Noise in Photomultiplier Tubes." Electro-
        Technology, LXXVIII (August, 1966), 56-58.

(14) Pilot Chemical, Inc. "Scintillation Grade Fluors Pilot
        Plastic Scintillators." Bulletin 622. Watertown,
        Massachusetts: Pilot Chemical, Inc., 1962.

(15) Saha, M. N., and B. N. Srivastava. A Treatise on Heat.
        4th ed. Calcutta, India: The Indian Press,
        Private Ltd., 1958.

(16) Robinson, R. A., and R. H. Stokes. Electrolyte Solu-
        tions. New York: Academic Press, Inc., 1955.

(17) Strickland, A. C., ed. Reports on Progress in Physics.
        London: The Institute of Physics and the Physical
        Society, 1966. Vol. XXIX. (Note "Plasma
        Spectroscopy" by J. Cooper.)

(18) Brown, Vernon D., and F. C. Todd. "Discussion of
        Radiation Intensity from a Vacuum Condenser Spark
        Between Aluminum Electrodes." Proceedings of the
        Oklahoma Academy of Science, XLVII, December,
        1967. (In print).

(19) Lengyel, Belo A. Introduction to Laser Physics. New
        York: John Wiley and Sons, Inc., 1966.

VITA

Vernon D. Brown

Candidate for the Degree of

Doctor of Education

Thesis: USE OF A PULSED PHOTOMULTIPLIER TO MEASURE THE
LIGHT INTENSITY VERSUS TIME FOR A SPARK DISCHARGE
BETWEEN ALUMINUM ELECTRODES

Major Field: Higher Education

Biographical:

Personal Data: Born in Batesville, Arkansas, August 15,
1934, the son of Granville G. and Hattie Jane
Brown.

Education: Graduated from Manila High School, Manila,
Arkansas, 1952; received Bachelor of Science
degree from Arkansas State College, with a major
in mathematics in August, 1959. Received the
Master of Arts degree from Marshall University,
with a major in Physical Science, in August, 1965.
Complete requirements for the Doctor of Education
degree in May, 1968.